

**This is the accepted manuscript version of the contribution published as:**

Schneider, J., Struve, M., **Trommler, U.**, Schlüter, M., Seidel, L., Dietrich, S., Rönsch, S.  
(2018):

Performance of supported and unsupported Fe and Co catalysts for the direct synthesis of  
light alkenes from synthesis gas

*Fuel Process. Technol.* **170** , 64 – 78

**The publisher's version is available at:**

<http://dx.doi.org/10.1016/j.fuproc.2017.10.018>

# 1 Performance of supported and unsupported Fe and Co catalysts for the direct 2 synthesis of light alkenes from synthesis gas

3 Jens Schneider<sup>1,\*</sup>, Marlen Struve<sup>1</sup>, Ulf Trommler<sup>2</sup>, Michael Schlüter<sup>1</sup>, Lisa Seidel<sup>1</sup>, Sebastian Dietrich<sup>1</sup>, Stefan  
4 Rönsch<sup>1,3</sup>

5 <sup>1</sup> *Syngas Technologies, DBFZ Deutsches Biomasseforschungszentrum gemeinnützige GmbH (the German  
6 Centre for Biomass Research), Torgauer Str. 116, 04347 Leipzig, Germany*

7 <sup>2</sup> *Department of Environmental Engineering, Helmholtz Centre for Environmental Research – UFZ,  
8 Permoserstr. 15, 04318 Leipzig, Germany*

9 <sup>3</sup> *Department of Industrial Engineering, Ernst-Abbe-Hochschule Jena, Carl-Zeiss-Promenade 2, 07745  
10 Jena, Germany*

11 \* Corresponding author. Tel.: +49 341 2434 382; Fax: +49 341 2434 133. E-mail address: Jens.Schneider@dbfz.de

## 12 Abstract

13 A sustainable way to produce plastics made from biomass (biomass to gas) and electricity (power to gas)  
14 could be obtained by the direct synthesis of light alkenes. Samples ( $\leq 1$  g) of the bulk catalysts Co/Fe,  
15 Fe/Na/S and the supported catalysts Fe/Mn|MgO and Co|SiO<sub>2</sub> are mentioned in the literature to allow the  
16 direct synthesis of light alkenes. These materials are studied in extended fixed beds with catalyst amounts  
17 between 35 and 70 g and classic syngas (H<sub>2</sub> and CO) in this work in order to prepare a potential scale-up of  
18 this technology.

19 The influence of activation conditions (H<sub>2</sub> or CO as reduction agent; 350 or 420 °C at 1.5 bar) and synthesis  
20 temperature (230 – 500 °C) on catalyst activity and product selectivity are pointed out. Selectivities to ethene  
21 of up to 11 % are found for Fe/Mn|MgO at  $T \approx 440$  °C and for Fe/Na/S at  $T \approx 310$  °C. The other materials did  
22 not produce significant amounts of ethene. CO<sub>2</sub> and CH<sub>4</sub> were the main products in any case, while C<sub>2</sub>H<sub>6</sub> was  
23 the main C<sub>2</sub> product. Applying CO as reduction agent was superior to activation with H<sub>2</sub> at low times on

1 stream (< 20 h). This is justified by the fast formation of carbides with CO as reduction agent since they are  
2 the most catalytically active species on Fe catalysts. The low selectivities observed for ethene are likely  
3 caused by the low GHSV value of 160 h<sup>-1</sup> applied in this study, which facilitates the conversion of primary  
4 alkenes in secondary reactions. Recommendations on operational conditions of Fischer-Tropsch to olefins  
5 processes are specified.

## 6 **Keywords**

7 Synthesis, Ethene, Propene, Fischer-Tropsch, Olefins, Syngas

8

## 9 **1 Introduction**

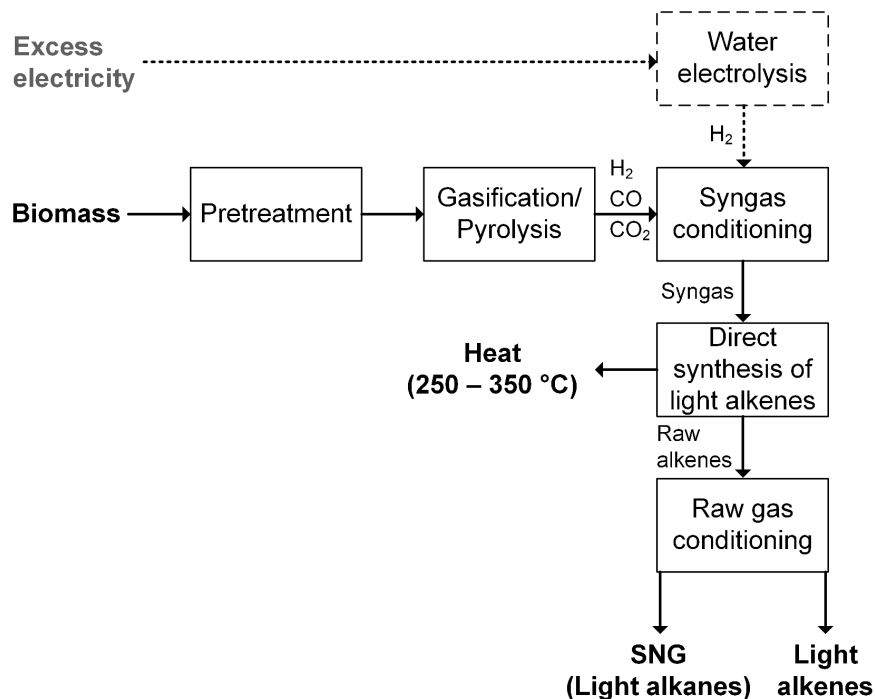
### 10 1.1 Background

11 Iron and cobalt catalysts are applied in several commercial Fischer-Tropsch plants in South Africa, ~~and~~ the  
12 Middle East and China that convert coal and natural gas in different reactor concepts [1,2]. The low-  
13 temperature approach (200 – 240 °C) targets at waxes as main products, whereas the high-temperature  
14 approach (300 – 350 °C) favors the formation of gasoline and diesel [3,4].

15 Besides these target products, light alkenes are of interest since they represent high-value bulk commodities  
16 with increasing demand of the plastic and chemical industry [5]. Light alkenes like ethene and propene show  
17 the highest production amounts of all organic chemicals [5]. More than half of the global plastic production  
18 capacity of about 300 million tons per year is based on these monomers [6]. But only below 1 % of the raw  
19 materials used for recent global plastic production originate from biomass [6,7].

20 The direct synthesis of light alkenes (Fischer-Tropsch to olefins) represents a process, which has not been  
21 commercialized yet and can produce light alkenes explicitly from biomass. Thermo-chemical pre-treatments,  
22 e. g. pyrolysis and gasification, are necessary for syngas provision. Besides that, methanol to alkenes  
23 synthesis, Fischer-Tropsch synthesis including cracking of Fischer-Tropsch products and oxidative coupling  
24 of methane [8–11] are commercialized processes, which target at the production of light alkenes but start  
25 with coal or natural gas as feedstock.

1 A principle process scheme is demonstrated in Fig. 1. Excess electricity can be exploited by water  
 2 electrolysis for hydrogen provision, which is especially needed for the fermentation path. Separation of  
 3 alkenes and alkanes might be conducted by pressure swing adsorption with silver zeolite A [12] or silver  
 4 nitrate dispersed on aluminosilica or clay [13].



5  
 6 Fig. 1: Simplified process scheme for the conversion of biomass into light alkenes with SNG as byproduct. Hydrogen  
 7 provision, e.g. by water electrolysis, is optional.

8 In order to facilitate the application of new catalysts in pilot scale, studies of catalysts in microreactors [14]  
 9 or small fixed beds with catalyst amounts of 1 g and below are the first step. Process conditions like catalyst  
 10 temperature and gas composition can be set easily in such setups. In contrast, fixed beds of decimeter and  
 11 larger sizes are characterized by distinct gradients of temperature and gas composition since these quantities  
 12 change steadily along the direction of gas flow. Problems like hot spots, reactor blocking due to coke  
 13 formation and altered gas compositions due to undesired reactions of the product gas with the catalyst at the  
 14 bottom end of a fixed bed are rarely taken into account in studies with very low catalyst amounts.

## 1 1.2 Aim of this study

2 It is the goal of this work to point out the influence of activation and process conditions on CO conversion  
3 and product selectivities for different Fe and Co test materials in an extended fixed bed. Promising  
4 combinations of catalyst and process conditions are expected from that.

5 A 41 cm long fixed-bed reactor with ten internal thermocouples and external heating is applied for synthesis  
6 studies. Between 35 and 70 g of catalyst are placed in this reactor with a distinct temperature profile.  
7 Different catalytically active materials are provided by an industrial catalyst manufacturer. The calcined  
8 catalysts are studied regarding their CO hydrogenation and alkene synthesis abilities at 230 – 500 °C, 1.4 – 2  
9 bar, H<sub>2</sub>/CO ratios of 3 and 1, and gas hourly space velocity (GHSV) = 160 h<sup>-1</sup>.

10 A background on the direct synthesis of light alkenes is given in chapter Background on the direct synthesis  
11 of light alkenes. Experimental conditions applied and the procedure for data evaluation is presented in  
12 chapters Experimental and Calculation of educt conversion and product selectivity. Results and a discussion  
13 of them are given in chapters Results and Discussion of the results. Summary and conclusions follow in  
14 chapter Another evaluation is done based on reaction velocities (Eq. 9 and Eq. 10). Eq. 9 is valid for the  
15 volume-based reaction rate and takes the difference in the molar concentration of CO between inlet and  
16 outlet  $\Delta c_{\text{CO}}$  as well as the contact time of the gas with the catalyst  $\Delta t$  into account. Eq. 10 represents the  
17 reaction rate based on the mass of iron and cobalt in each test material  $m_{\text{Fe,Co}}$ .  $f_{\text{Fe,Co}}$  represents the  
18 fraction of Fe and Co in a test material in Eq. 10.  $\Delta t$  is equivalent to the quotient of the bed volume  $V_{\text{bed}}$  and  
19 the volumetric flow rate so that the right formula of Eq. 10 can be applied with known values. The cases  
20 with the highest yields to C<sub>2</sub> products from Table 12 are compared in Table 13 with the help of the mass-  
21 bases reaction rate (Eq. 10). The reaction rate to C<sub>2</sub> products is quoted as well..

## 22 **2 Background on the direct synthesis of light alkenes**

### 23 2.1 Basic process conditions

24 This process receives increased attention since the 1980's and could accelerate the still slow substitution of  
25 fossil-based plastics by biomass-based. Torres Galvis and de Jong published a review about catalysts for the  
26 direct thermo-chemical production of light alkenes from synthesis gas in 2013 [11]. Results about many

1 supported and unsupported catalysts, of which most are on the basis of iron and/or cobalt, are summarized by  
2 them. Temperatures and pressures studied by most authors vary between 250 – 450 °C and 1 – 25 bar at  
3 H<sub>2</sub>/CO ratios of 1 – 3. At these conditions, maximum selectivities to C<sub>2</sub> – C<sub>4</sub> alkenes are expected, while  
4 methane, carbon dioxide, and water represent major byproducts [11]. Lower amounts of C<sub>2</sub> – C<sub>4</sub> alkanes, C<sub>5</sub>+  
5 hydrocarbons as well as oxygenated hydrocarbons are produced additionally. Zohdi-Fasaei et al. found  
6 optimal conditions for light alkene synthesis at 312 °C, 2 bar, H<sub>2</sub>/CO = 1 and GHSV = 4500 h<sup>-1</sup> with a  
7 Co/Mn/Ce/SiO<sub>2</sub> catalyst [15].

8 Several studies have shown that the activation conditions like reduction agent (H<sub>2</sub>, CO or H<sub>2</sub> and CO) and  
9 temperature have major influence on catalyst activity and selectivity to light alkenes with Fe [16–19]. This is  
10 mostly attributed to the formation of different iron carbides like ε'-Fe<sub>2.2</sub>C, χ-Fe<sub>2.5</sub>C, and θ-Fe<sub>3</sub>C, which are the  
11 active phases responsible for the formation of hydrocarbon products with two or more carbon atoms and can  
12 convert into each other under certain conditions [16–20].

13 Beside the process conditions, the catalyst applied plays a major role. Unsupported or bulk catalysts for the  
14 direct synthesis of light alkenes show a low mechanical stability due to carbon deposition or density  
15 differences between oxidic and carbidic phases [11,19,21]. These problems might be overcome by reducing  
16 the size of the active material to the range of nanometers, which can be induced with the help of a supporting  
17 material. Agglomeration of particles of the active material is reduced in this way, so that the formation of  
18 carbon depositions and the fragmentation of individual catalyst particles is reduced or inhibited [11,22].

19 From the list of catalysts reviewed by Torres Galvis and de Jong [11], two supported and two unsupported  
20 examples, which showed high alkene selectivities at high CO conversions, are selected and studied in this  
21 work. The results of these studies in small reactors are presented in the following.

## 22 2.2 Selected studies with bulk and supported catalysts

### 23 2.2.1 Co/Fe bulk catalyst

24 Mirzaei et al. prepared and studied an unsupported catalyst that contained ca. 47 wt% cobalt, 28 wt% iron, 4  
25 wt% silicon and 21 wt% oxygen with small amounts of potassium [23]. It is made by co-precipitation of

1 aqueous solutions of the hydrates of cobalt and iron nitrate, silica powder and potassium nitrate. Synthesis  
2 experiments are performed with 1 g of meshed material in a fixed-bed reactor at 1 bar, temperatures between  
3 350 and 500 °C, H<sub>2</sub>/CO ratios of 1 – 4, and GHSV of 4050 – 5400 h<sup>-1</sup>. CO conversions are > 80 % with C<sub>2</sub>H<sub>4</sub>  
4 selectivities between 8 % (H<sub>2</sub>/CO = 1) and 30 % (H<sub>2</sub>/CO = 4) as well as C<sub>3</sub>H<sub>6</sub> selectivities between 26 %  
5 (H<sub>2</sub>/CO = 1) and 23 % (H<sub>2</sub>/CO = 4) [23]. Other products like CH<sub>4</sub>, H<sub>2</sub>O, CO<sub>2</sub> seem to have not been taken  
6 into account, which explains the extraordinarily high selectivities mentioned. It was reported that the Co/Fe  
7 catalyst kept its activity and selectivity in a 72 h test at the best operation conditions (450 °C, H<sub>2</sub>/CO = 4,  
8 GHSV = 5400 h<sup>-1</sup>) [23].

### 9 2.2.2 Fe/Na/S bulk catalyst

10 Botes et al. modified an iron catalyst of Sasol promoted with sodium and sulphur that showed a high affinity  
11 for C<sub>2</sub> – C<sub>4</sub> products (mainly alkenes) and a low methane selectivity (< 15 %) at a CO conversion to  
12 hydrocarbons of 40 % [24]. Five non-metal promoters namely boron, phosphorous, sulphur, chlorine and  
13 antimony are combined with sodium or potassium. Amounts between 0.4 and 5 mmol of non-metal  
14 promoters and between 1.6 and 25 mmol of alkali promoters are added to 1.78 mol (100 g) of iron in the  
15 form of iron(III) nitrate. In total, 306 catalysts are prepared and tested in an Avantium Nanoflow catalyst  
16 testing unit. 15 catalysts with sizes of 38 – 150 µm (25 mg) are tested in parallel. The catalysts are activated  
17 with H<sub>2</sub> at 420 °C and 20 bar for 16 hours. Hydrocarbon synthesis conditions are set to 330 °C, 20 bar, educt  
18 gas composition of 57 vol% H<sub>2</sub>, 14 vol% CO and 11 vol% CO<sub>2</sub> with He in balance and a flow rate of 12.9 L  
19 (g h)<sup>-1</sup> (NTP) [24]. The latter approximates a GHSV of 320 h<sup>-1</sup>. Synthesis products are measured by gas  
20 chromatography with thermal conductivity detector (GC-TCD), GC with flame ionization detector (GC-FID)  
21 and GC with mass spectrometry (GC-MS). The combination of sodium and sulphur yielded the highest  
22 selectivities to C<sub>2</sub> – C<sub>4</sub> alkenes with low methane selectivities relative to all other combinations. A molar  
23 Na/S ratio of about two is recommended to yield the highest C<sub>2</sub> – C<sub>4</sub> selectivities (~ 65 %) [24]. Furthermore,  
24 it is pointed out that the selectivity to C<sub>2</sub> – C<sub>4</sub> products decreases when the CO conversion to hydrocarbons  
25 increases above 30 %.

### 1 2.2.3 Fe/Mn/K|MgO supported catalyst

2 Different catalytic supports with iron and manganese(II) oxide are studied by Xu et al. in regard to the  
3 production of light alkenes from synthesis gas [25]. MgO, ZrO<sub>2</sub>, TiO<sub>2</sub>, Al<sub>2</sub>O<sub>3</sub> and SiO<sub>2</sub> particles with sizes  
4 between 20 and 30 mesh (0.60 – 0.84 mm) are impregnated with Fe and Mn salt solutions for catalyst  
5 preparation. CO hydrogenation studies with 1 ml of calcined catalysts with different support are conducted  
6 with synthesis gas at 277 – 347 °C, 10 – 20 bar, H<sub>2</sub>/CO = 2, and GHSV = 500 – 3000 h<sup>-1</sup> in a microreactor.  
7 Products are studied with a GC-TCD. CO conversion and the distribution of alkanes and alkenes up to C<sub>4</sub> are  
8 reported. The best selectivity to C<sub>2</sub> – C<sub>4</sub> alkenes are observed with MgO as support. The Fe/Mn/MgO catalyst  
9 remained a CO conversion of 78.6 % and a selectivity to C<sub>2</sub> – C<sub>4</sub> alkenes as high as 68.3 % (nearly equal  
10 distribution of ethene, propene and butene) after 1000 h on stream [25]. Selectivities to light alkenes  
11 increased with temperature up to 317 °C together with CO conversion and increased with space velocity up  
12 to 2000 h<sup>-1</sup> at decreasing CO conversion [25]. Furthermore, Xu et al. studied the promotion effect of  
13 potassium(I) oxide and manganese(II) oxide and found maximum values for the selectivity to light alkenes  
14 and CO conversion when both promoters were present on an iron silicalite-2 catalyst [26]. Based on these  
15 results, iron supported on magnesium(II) oxide and promoted with manganese and potassium seems to be a  
16 promising supported catalyst for the synthesis of light alkenes.

### 17 2.2.4 Co|SiO<sub>2</sub> supported eggshell catalyst

18 Iglesia et al. produced cobalt catalysts supported on silica spheres with uniform distribution of cobalt and  
19 increased concentrations of cobalt in the outer shell [27]. The term eggshell catalysts refer to the latter case.  
20 Silica spheres with a diameter of 2.2 mm are contacted with solutions of cobalt nitrate (0.5 g cm<sup>-3</sup>) or cobalt  
21 nitrate melts (at 60 – 75 °C) for a few seconds with subsequent removal of the liquid. Catalysts with uniform  
22 Co distribution are prepared by incipient wetness impregnation of silica spheres with aqueous cobalt nitrate  
23 solutions. Besides that, powders with uniform Co distribution are prepared by mixing silica pellets with a  
24 diameter of 0.14 mm and cobalt nitrate in acetone. Catalysts are reduced in hydrogen at 435 – 450 °C.  
25 Synthesis studies are performed in isothermal packed beds diluted with quartz powder at 200 °C, 20 bar and

1 H<sub>2</sub>/CO ratios of 2.0 – 2.1. It is shown that eggshell catalysts have higher conversion rates, higher selectivities  
2 to C<sub>5+</sub> products, higher selectivities to alkenes, lower selectivities to CH<sub>4</sub> and lower selectivities to CO<sub>2</sub> than  
3 catalysts of comparable size and total Co loading but uniform Co distribution [27].

### 4 **3 Experimental**

#### 5 3.1 Catalyst preparation

6 The following catalysts ~~are~~were produced by an industrial catalyst manufacturer based on the descriptions  
7 below and of the references cited. The compositions obtained are~~is~~ presented in section Catalyst  
8 characterization.

##### 9 3.1.1 Co/Fe based on [23]

10 Aqueous solutions of Co(NO<sub>3</sub>)<sub>2</sub> · 6H<sub>2</sub>O (0.5 mol l<sup>-1</sup>) and Fe(NO<sub>3</sub>)<sub>3</sub> · 9H<sub>2</sub>O (0.5 mol l<sup>-1</sup>) were premixed in the  
11 molar ratio 60:40 and heated to 70 °C. 15 wt% SiO<sub>2</sub> powder were added to the solution of Co and Fe nitrates.  
12 The amount of additives corresponds to the mass of the solution. An aqueous solution of Na<sub>2</sub>CO<sub>3</sub> (0.5 mol l<sup>-1</sup>)  
13 was added to the aforementioned solution with stirring at 70 °C until a pH value of 7.0 was reached. The  
14 resulting precipitate was left in the medium for 2 h. The precipitate was filtered out of the medium, washed  
15 with warm distilled water until no Na<sup>+</sup> ions were present in the washing water and dried at 110 °C for 18 h.  
16 This precursor was impregnated with an appropriate amount of aqueous KOH. The resulting precursor was  
17 dried at 110 °C again and calcined in static air at 600 °C for 2 h.

##### 18 3.1.2 Fe/S and Fe/Na/S based on [24]

19 An aqueous solution of Fe(NO<sub>3</sub>)<sub>3</sub> (1 mol l<sup>-1</sup>) was vigorously stirred at room temperature and a 25 wt%  
20 solution of NH<sub>4</sub>OH was added until a pH value of 6.0 was reached. Appropriate amounts of aqueous  
21 (NH<sub>4</sub>)<sub>2</sub>SO<sub>4</sub> (for Fe/S) and Na<sub>2</sub>CO<sub>3</sub> (for Fe/Na/S) were added to the resulting precipitate as promoters. This  
22 precursor was washed and dried for 12 h at 150 °C and calcined at 350 °C in static air for 4 h.

### 1 | 3.1.3 Fe|MgO and Fe/Mn|MgO based on [25,26]

2 | MgO was impregnated with an aqueous solution of  $\text{Fe}(\text{NO}_3)_3 \cdot 9\text{H}_2\text{O}$  (10 wt% Fe) for Fe|MgO or with an  
3 | aqueous solution containing  $\text{Fe}(\text{NO}_3)_3 \cdot 9\text{H}_2\text{O}$  (7 wt% Fe) and  $\text{Mn}(\text{NO}_3)_2 \cdot 4\text{H}_2\text{O}$  (7 wt% Mn). The resulting  
4 | precursors were dried at 105 °C for 12 h and calcined at 450 °C for 3 h.

### 5 | 3.1.4 Co|SiO<sub>2</sub> based on [27]

6 | SiO<sub>2</sub> was impregnated with an aqueous solution of  $\text{Co}(\text{NO}_3)_2$  (13 wt% Co). The resulting precursor was dried  
7 | in air at 105 °C overnight and calcined in air at 350 °C for 3 h.

- 8 | • Co/Fe bulk catalyst [23],  
9 | • Fe/Na/S bulk catalyst [24],  
10 | • Fe|MgO and Fe/Mn|MgO supported catalysts [25,26] and  
11 | • Co|SiO<sub>2</sub> supported eggshell catalyst [27].

12 | ~~All catalysts used in this study are produced by an industrial manufacturer with the help of standard in-house~~  
13 | ~~methods. Nitrate salts of the active materials are used in aqueous solution. Low or high amounts of a~~  
14 | ~~pulverized support are added prior to precipitation. The precipitates are dried and subsequently calcined at~~  
15 | ~~350—450 °C for several hours. Samples are provided to the DBFZ for further studies.~~ The composition  
16 | obtained is presented in section Catalyst characterization.

## 17 | 3.2 Catalyst characterization

### 18 | 3.2.1 Physical adsorption

19 | BET surface areas, pore volumes, and average pore diameters of calcined test materials are determined by N<sub>2</sub>  
20 | physisorption at 77 K. 0.1 – 0.4 g of each material is degassed at 100 °C for 1 h, heated to 300 °C at 10 K  
21 | min<sup>-1</sup> and held at this temperature for at least 10 h before BET analysis.

### 22 | 3.2.2 Catalyst composition

23 | X-ray fluorescence spectroscopy (XRF) is applied to determine the elemental composition of the test  
24 | materials.

### 1 3.2.3 Temperature-programmed reduction (TPR)

2 0.2 g of calcined test materials are used to determine their reduction behavior. The samples are treated with 5  
3 vol% H<sub>2</sub> in Ar or with 5 vol% CO in He at a flow rate of 50 ml min<sup>-1</sup>. A heating rate of 10 K min<sup>-1</sup> is used. A  
4 maximum temperature of 1000 °C is set for H<sub>2</sub>. In case of CO, a maximum temperature of 600 °C is applied.  
5 Two thermal conductivity detectors in differential mode are used to measure the consumption of H<sub>2</sub> or CO. A  
6 zeolite-based trap for H<sub>2</sub>O in case of H<sub>2</sub>-TPR or for CO<sub>2</sub> in case of CO-TPR is used during the reduction  
7 procedure.

### 8 3.2.4 Temperature-programmed oxidation (TPO)

9 Amount and composition of depositions on used catalyst samples are studied by TPO experiments. Used  
10 catalysts are passivated with 0.2 L min<sup>-1</sup> (STP) of flowing air at room temperature, while the temperature in  
11 the fixed bed is observed in order to keep it below 50 °C. Used passivated catalyst samples are placed into a  
12 thermo-gravimetric analyzer and heated up to 900 °C in flowing synthetic air. A qualitative evaluation of  
13 their coverage with carbonaceous species is conducted based on these TPO experiments in section Reactor  
14 pressure increase due to the formation of carbonaceous species.

## 15 3.3 Synthesis studies

### 16 3.3.1 Experimental setup

17 The experimental setup consists of a cylindrical reactor, which includes the fixed bed and is heated  
18 externally by an oven (Fig. 2). Permanent gases (N<sub>2</sub>, CO, H<sub>2</sub>) and water are provided by mass flow  
19 controllers (MFCs) and a HPLC-pump, respectively. These educts are heated up in the educt gas line to  
20 temperatures up to ca. 250 °C prior to entering the reactor. The product gas line is kept at a temperature of  
21 ca. 200 °C and leads to a gas chiller, where all non-permanent gas components are condensed at 3 °C. The  
22 dry product gas is directed to a gas analyzer (GC-TCD), recycled to the educt gas line or discharged via the  
23 chimney.

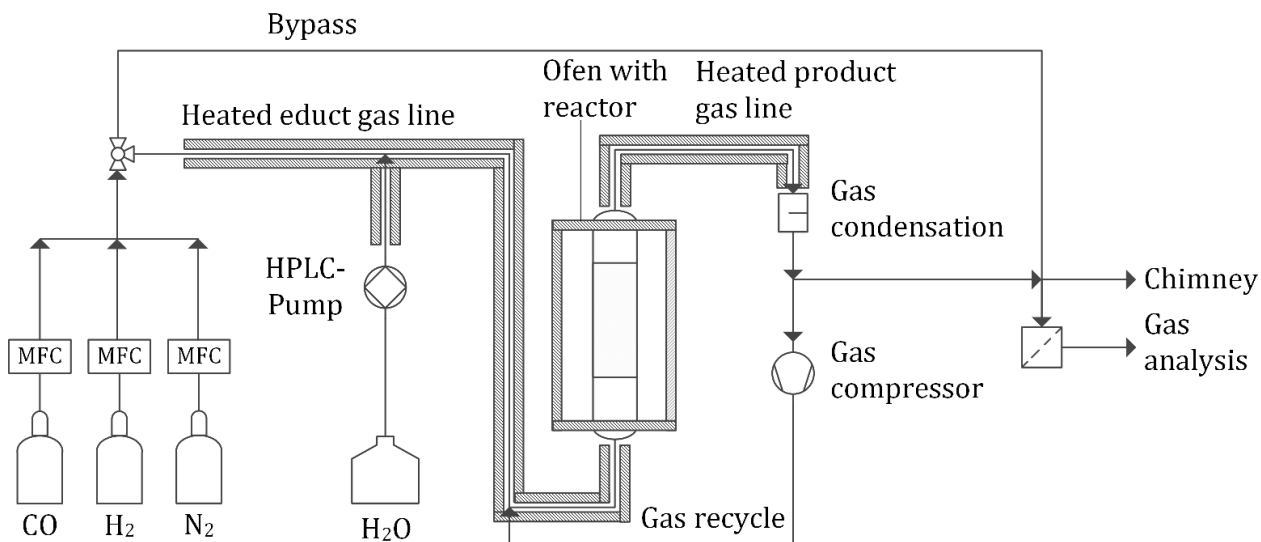


Fig. 2: Scheme of the experimental setup consisting of gas and steam supply, heated educt gas line, oven with fixed-bed reactor, heated product gas line, gas condensation, gas recycle and gas analysis

- 1 The cylindrical reactor containing the fixed bed is displayed in Fig. 3. It includes the fixed bed of catalytic
- 2 material in the center part (ca. 74 ml) and silica wool at in- and outlet. Furthermore, an inner tube is
- 3 positioned at the axis of the cylinder and contains ten thermocouples, which measure the temperature at
- 4 different positions. The actively heated part of the reactor is also outlined in Fig. 3. The remaining parts of
- 5 the reactor are insulated properly to reduce thermal losses.

- 6 [Synthesis studies were performed with 50.8 g of Fe|MgO, 58.3 g of Fe/Mn|MgO, 67.9 g of Co/Fe, 56.3 g of](#)
- 7 [Fe/S, 34.4 g of Fe/Na/S \(reactor was only partly filled\) and 40.3 g of Co|SiO<sub>2</sub>.](#)

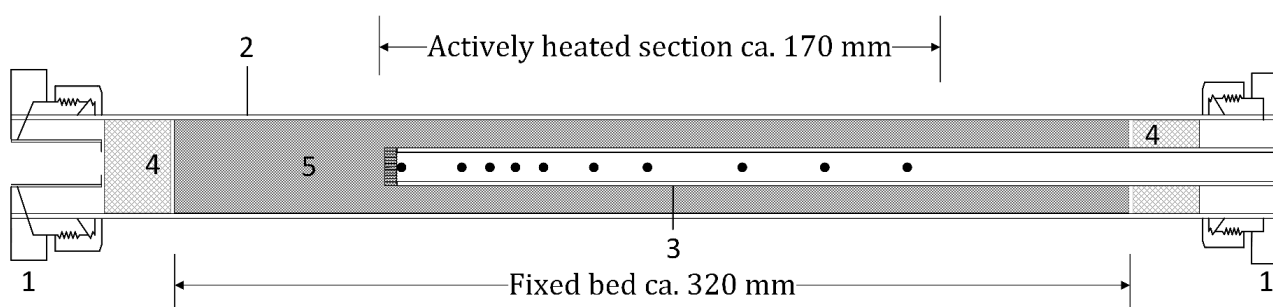


Fig. 3: Cross-sectional view of the reactor consisting of: (1) flanges, (2) steel tubing, (3) inner tube with ten thermocouples (marked by ●), (4) silica wool and (5) fixed catalytic bed.

### 1 3.3.2 Analysis of gaseous components

2 The product gas is cooled to 3 °C in a gas chiller for the removal of any condensable gas components prior to  
 3 gas analysis at room temperature. A GC-TCD is used for the detection of H<sub>2</sub>, N<sub>2</sub>, CO, CO<sub>2</sub>, CH<sub>4</sub>, C<sub>2</sub>H<sub>4</sub>, and  
 4 C<sub>2</sub>H<sub>6</sub>. The GC-TCD is of the type GCM Microbox II from the company Elster GmbH. It is calibrated daily  
 5 with test gases containing all relevant species.

### 6 3.3.3 Activation procedure

7 1 L min<sup>-1</sup> (STP) of N<sub>2</sub> for 10 min is used to remove impurities from the reactor prior to activation. 0.2 L min<sup>-1</sup>  
 8 (STP) of a reduction agent (80 vol% N<sub>2</sub> and 20 vol% H<sub>2</sub> or 80 vol% N<sub>2</sub> and 20 vol% CO) are applied for  
 9 activation starting from room temperature to different target temperatures (maximally 350 or 420 °C in the  
 10 fixed bed) with a heating rate of 10 K min<sup>-1</sup>. In order to reach a specific maximum temperature in the fixed  
 11 bed, the oven temperature is set 15 K higher. The dry product gas composition is measured every 5 min.

12 Reduction agent flow rate and composition as well as target temperature are kept constant for 5 – 6 hours  
 13 until H<sub>2</sub> and/or CO values in the product gas are close to their respective values in the educt gas. The reactor  
 14 is cooled down under 2 L min<sup>-1</sup> (STP) of flowing N<sub>2</sub> after completion of the activation procedure and kept at  
 15 room temperature at a pressure of 2 – 3 bar. The activation of Co/Fe catalysts is conducted with the addition  
 16 of ~ 0.04 g min<sup>-1</sup> (~ 16.7 vol%) of steam. Table 1 summarizes the conditions applied during different  
 17 activation and synthesis procedures.

18 Table 1: Conditions applied during activation and synthesis.

	Oven temperature in °C	Total flow rate in l/min (STP)	N <sub>2</sub>	H <sub>2</sub>	CO in vol%	H <sub>2</sub> O (steam)
Activation I	365	0.20	80	20	0	0
Activation II	365	0.20	80	0	20	0
Activation III	365	0.24	66.7	16.7	0	16.7
Activation IV	365	0.24	66.7	0	16.7	16.7
Activation V	435	0.20	80	20	0	0
Synthesis I	230 – 500	0.20	0	75	25	0
Synthesis II	230 – 500	0.20	0	50	50	0
Synthesis III	230 – 500	0.24	0	62.5	20.8	16.7
Synthesis IV	230 – 500	0.24	0	41.7	41.7	16.7

### 1 3.3.4 Synthesis of light alkenes at different temperatures

2 Activated catalysts are heated from room temperature to the target temperature (230 – 500 °C) under 1 l min<sup>-1</sup>  
3 (STP) flowing N<sub>2</sub>. After reaching the target temperature, the gas flow is switched to 0.2 l min<sup>-1</sup> (STP) of  
4 syngas (75 vol% H<sub>2</sub> and 25 vol% CO or 50 vol% H<sub>2</sub> and 50 vol% CO). The dry product gas composition is  
5 analyzed every 5 min with the GC-TCD. The conditions are kept constant until temperature distribution in  
6 the catalyst bed and gas composition are stable for at least four subsequent measurements.

7 Typically, a specific oven temperature is set at 75 vol% H<sub>2</sub> and 25 vol% CO. After reaching stable  
8 conditions, gas composition is changed to 50 vol% H<sub>2</sub> and 50 vol% CO. After reaching stable conditions  
9 again, oven temperature is increased by ca. 10 K with 75 vol% H<sub>2</sub> and 25 vol% CO. This procedure is  
10 continued until dry product gas concentrations are analyzed up to a temperature of 500 °C or until a  
11 significant pressure increase (0.5 – 1 bar) in front of the reactor is observed. Each catalyst is hold at a  
12 specific temperature for 40 – 80 min. A steady product gas composition is reached during the last 20 – 40  
13 min and the average concentration values of this interval are used for the calculation of conversions and  
14 selectivities. It is possible that slow changes in catalyst composition, which need between hours and a few  
15 days to be finalized [20,28], have taken place at synthesis temperatures which are significantly higher than  
16 the activation temperature. This is likely the case with Fe catalysts, when H<sub>2</sub> is used as reduction agent, since  
17 the catalytically active iron carbides form only if CO or CO<sub>2</sub> is present. Further activation of the catalyst bed  
18 at high synthesis temperatures can also have taken place if CO is used as reduction agent or with Co catalysts  
19 but to a minor extent. The global steady-state regime is not achieved since a time on stream of several days is  
20 needed for this.

21 Since measurements can only be performed during day time, the reactor is cooled down under 2 l min<sup>-1</sup>  
22 (STP) of flowing N<sub>2</sub> at the end of a day and kept at room temperature at a pressure of 2 – 3 bar during night  
23 time. Measurements with the same test material at higher temperatures are continued at the following days.

## 1 4 Calculation of educt conversion and product selectivity

### 2 4.1 Determination of the nitrogen-free gas composition

3 Experiments are carried out at low GHSV of ca.  $160 \text{ h}^{-1}$  (catalyst volume ca. 74 ml) in order to reach high  
 4 product concentrations. Dry product gas flow rates can be below  $0.1 \text{ l min}^{-1}$  (STP) in this way especially at  
 5 high educt conversions. Since the GC-TCD consumes a certain amount of product gas per measurement, air  
 6 can be sucked into the GC-TCD via the tube leading to the chimney. This leads to dilution of the dry product  
 7 gas by air so that the measured concentration of the other species appears to be lower. Furthermore,  $\text{H}_2$   
 8 concentrations above ca. 43 vol% cannot be quantified accurately since the detector signal is too high in this  
 9 case.

10 In order to approximate the real concentrations  $y_r$  with the help of the apparent concentrations  $y_a$  in the dry  
 11 product gas, Eq. 1 and Eq. 2 are applied. In these equations, the index  $g$  represents a variable for the gas  
 12 species  $\text{CO}$ ,  $\text{CO}_2$ ,  $\text{CH}_4$ ,  $\text{C}_2\text{H}_4$  and  $\text{C}_2\text{H}_6$ . The concentration for  $\text{H}_2$  is calculated in the form of a balance (Eq. 2)  
 13 since no other detectable species can be present. A value for  $\text{H}_2$  can be quoted in this way in any case though  
 14 its concentration might be overestimated.

Eq. 1

Eq. 2

### 15 4.2 Approximation of conversion and selectivity

16 Eq. 3 and Eq. 4 are applied in order to calculate educt conversions  $X_h$  (index  $h$  for  $\text{CO}$  and  $\text{H}_2$ ) and product  
 17 selectivities  $S_i$  (index  $i$  for  $\text{CO}_2$ ,  $\text{CH}_4$ ,  $\text{C}_2\text{H}_4$ ,  $\text{C}_2\text{H}_6$ ) based on  $\text{CO}$ . The stoichiometric coefficients of a certain  
 18 component in a chemical reaction are indicated by  $\nu_i$ . While the molar flow rate is known for the educts, it is  
 19 unknown for the products. In order to solve this problem, it is assumed that a number  $\beta$  exists (volume  
 20 reduction), which connects the molar flow rates of educt and product gas according to Eq. 5. A carbon  
 21 balance is formulated (Eq. 6). The solver `fzero` is applied with the help of the free software GNU Octave to  
 22 find the right value for  $\beta$ . Molar flow rates of the products measured are calculated by Eq. 5, while it is  
 23 assumed that volumetric concentrations are identical with molar concentrations.

Eq. 3

Eq. 4

Eq. 5

1 The methodology described yields significant errors. Selectivities are overestimated since not all possible  
2 products are quantified. Especially  $C_3$  and  $C_4$  hydrocarbons are not measured by the GC-TCD applied.  
3 Liquid hydrocarbons ( $C_{5+}$ ), carboxylic acids and alcohols are condensed together with water in the cooler  
4 (gas condensation in Fig. 2). Their concentrations could not be quantified for each individual process  
5 condition. But the share of alcohols and carboxylic acids in the liquid phase is below 1 wt% in the cases,  
6 where the liquid phase was analyzed. It is assumed that their concentrations can be neglected at the  
7 conditions studied. No or very low amounts of oily phases on top of the liquid phase are observed indicating  
8 low selectivities to or the absence of  $C_{5+}$  hydrocarbons in the wet product gas.

9

## 10 **5 Results**

### 11 5.1 Catalyst characterization

12 The results of XRF analyses of the catalysts applied are compared to the compositions published by Xu et al.  
13 [25,26], Mirzaei et al. [23], Iglesia et al. [27] and Botes et al. [24] in Table 2. While Xu et al. studied Fe with  
14 nearly equal amounts of Mn and K on MgO [25] and silicalite-2 [26], our test materials contained Fe or Fe  
15 and Mn on MgO for comparison. The composition of Mirzaei et al. is reproduced well containing the main  
16 components Co and Fe in amounts differing to below 3.5 wt%. The composition of Botes et al. is reproduced  
17 according to the procedure published [24]. The Co|SiO<sub>2</sub> test material studied contained 20 wt% Co, while  
18 Iglesia et al. applied eggshell catalysts with ca. 13 wt% Co on silica carriers.

19 The surface properties of the different test materials are displayed in Table 3. BET surface areas varied  
20 between 53 and 154 m<sup>2</sup> g<sup>-1</sup>. Co/Fe has the highest surface area though it contains only 2.5 wt% Si as silica  
21 and is considered as bulk catalyst. In contrast, Fe/S includes no support at all and shows the lowest surface  
22 area. Pore volumes typically vary between 0.2 and 0.4 cm<sup>3</sup> g<sup>-1</sup>. Only Co|SiO<sub>2</sub> shows a higher value of 0.7 cm<sup>3</sup>  
23 g<sup>-1</sup>. All test materials are mesoporous with narrow pore distributions. Only Co|SiO<sub>2</sub> shows a wide pore  
24 distribution.

1 Table 2: Elemental composition of the calcined catalysts in wt% produced by Xu et al. [25,26], Mirzaei et al. [23],  
 2 Botes et al. [24] and Iglesia et al. [27] as well as the respective values for the test materials supplied by an industrial  
 3 catalyst manufacturer.

Catalyst	Fe	Mn	K	Co	Mg	Si	O	Na	S
Xu et al.	9.5	9.6	8.3	-	-	n.s.	n.s.	-	-
Fe MgO	8.7	-	-	-	52.9	-	38.4	-	-
Fe/Mn MgO	9.3	9.3	-	-	36.2	-	45.2	-	-
Mirzaei et al.	28.2	-	0.2	46.9	-	3.5	21.2	-	-
Co/Fe	27.0	-	0.14	43.4	-	2.5	26.5	-	-
Botes et al. <sup>1</sup>	69.3	-	-	-	-	-	29.9	~ 0.003	~ 0.002
Fe/S	69.3	-	-	-	-	-	29.9	-	~ 0.002
Fe/Na/S	69.3	-	-	-	-	-	29.9	~ 0.003	~ 0.002
Iglesia et al.	-	-	-	~ 13.0	-	39.06	47.94	-	-
Co SiO <sub>2</sub>	-	-	-	13.0	-	39.1	47.9	-	-

4 <sup>1</sup> Calculated for Na and S loadings of 10 mmol and 5 mmol, respectively

5 Table 3: BET surface area, pore volume and pore diameters of the calcined catalysts produced by an industrial catalyst  
 6 manufacturer

Catalyst	BET surface area in m <sup>2</sup> g <sup>-1</sup>	Pore volume in cm <sup>3</sup> g <sup>-1</sup>	Pore diameter range in nm
Fe MgO	62.5	0.30	2 – 30
Fe/Mn MgO	135.0	0.39	2 – 12
Co/Fe	153.9	0.27	2 – 7
Fe/S	53.4	0.19	4 – 12
Co SiO <sub>2</sub>	87.1	0.70	1 – 90

7  
 8 Fig. 4 shows the TPR profiles for all tested materials (A/C: Fe|MgO, Fe/Mn|MgO, Fe/S; B/D: Co|SiO<sub>2</sub>,  
 9 Co/Fe) reduced with H<sub>2</sub> (A/B) or CO (C/D). The related peak temperatures of different reduction steps are  
 10 shown in Table 4 and Table 5. The relation of peak reduction temperatures and reduction steps are based on  
 11 [29,30].

12 The analysis of the reduction temperatures allows several conclusions. At first, the usage of CO instead of H<sub>2</sub>  
 13 significantly shifts the peak reduction temperatures towards lower values, since CO is the stronger reduction  
 14 agent. The shift ranges from 34 K to 183 K for the iron-based catalysts (A/C) and from -4 K to 65 K for the  
 15 cobalt-based catalysts (B/D). Therefore, at the same given reduction temperature of 350 °C, a catalyst  
 16 reduced by CO is expected to be more active than the same catalyst reduced by H<sub>2</sub>.

1 Comparing the bulk catalyst Fe/S with the supported iron-catalysts shows that the reduction temperature of  
 2 iron shifts towards lower temperatures for the first step ( $\text{Fe}_2\text{O}_3 \rightarrow \text{Fe}_3\text{O}_4$ ) and towards higher temperatures for  
 3 the second one ( $\text{Fe}_3\text{O}_4 \rightarrow \text{FeO}$ ), when CO instead of  $\text{H}_2$  is used as reduction agent. The latter is even more  
 4 pronounced. In case of the Co catalysts, the reduction temperatures of cobalt generally shift towards lower  
 5 temperatures if Co is supported on  $\text{SiO}_2$  and not part of the Co/Fe bulk phase.

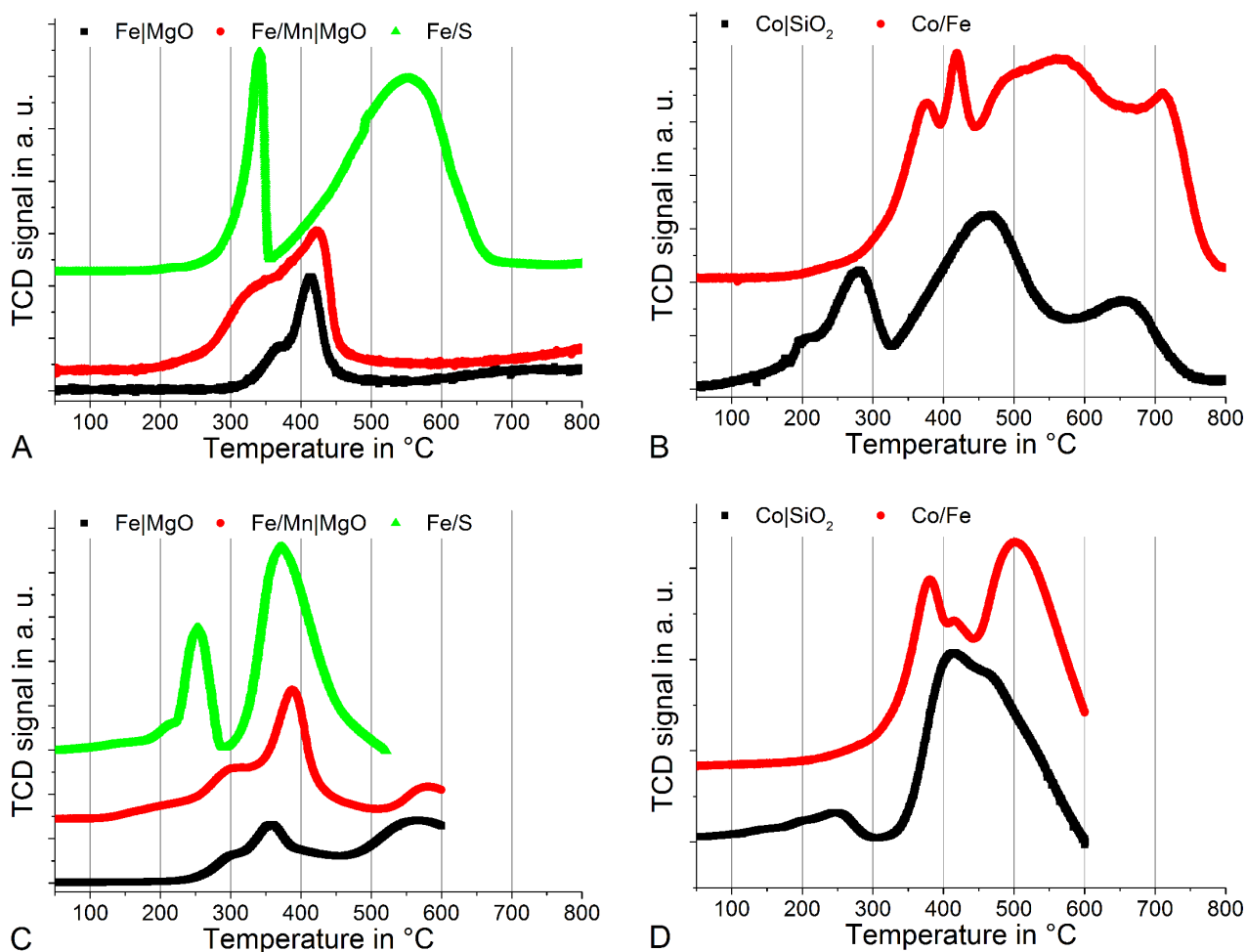


Fig. 4: TPR profiles for all test materials using  $\text{H}_2$  (A, B) or CO (C, D) as gasification agent. A, C: for Fe|MgO, Fe/Mn|MgO and Fe/S. B, D: for Co/Fe and Co|SiO<sub>2</sub>.

6 Table 4: Peak temperatures of different reduction steps observed for Fe|MgO, Fe/Mn|MgO and Fe/S with  $\text{H}_2$  or CO as  
 7 reduction agent (compare Fig. 4).

Reduction step	Related temperature in °C					
	A ( $\text{H}_2$ )			C (CO)		
	Fe MgO	Fe/Mn MgO	Fe/S	Fe MgO	Fe/Mn MgO	Fe/S

$\text{Fe}_2\text{O}_3 \rightarrow \text{Fe}_3\text{O}_4$	369	362	341	297	304	253
$\text{Mn}_2\text{O}_3 \rightarrow \text{MnO}$	-	362	-	-	304	-
$\text{Fe}_3\text{O}_4 \rightarrow \text{FeO}$	414	422	554	359	388	371
$\text{FeO} \rightarrow \text{Fe}$	710	> 800	-	566	581	-

1  
2  
3  
4  
5  
6  
7

8 Table 5: Peak temperatures of different reduction steps observed for Co|SiO<sub>2</sub> and Co/Fe with H<sub>2</sub> or CO as reduction  
9 agent (compare Fig. 4).

Reduction step	Related temperature in °C			
	B (H <sub>2</sub> )		D (CO)	
	Co SiO <sub>2</sub>	Co/Fe	Co SiO <sub>2</sub>	Co/Fe
$\text{Co}_3\text{O}_4 \rightarrow \text{CoO}$	279	376	248	380
$\text{Fe}_2\text{O}_3 \rightarrow \text{Fe}_3\text{O}_4$	-	376	-	380
$\text{Fe}_3\text{O}_4 \rightarrow \text{FeO}$	-	419	-	415
$\text{CoO} \rightarrow \text{Co}$	464	567	415	502
$\text{FeO} \rightarrow \text{Fe}$	-	711	-	-

10

## 11 5.2 Temperature distribution at activation and synthesis

12 Fig. 5 demonstrates the temperature distribution inside of the fixed-bed reactor during activation (A – B) and  
13 synthesis (C – D) at different oven temperatures for most of the test materials. A Gaussian function is applied  
14 to measured temperature values in order to approximate the temperature distribution at the front and rear part  
15 of the fixed bed. During activation with H<sub>2</sub> at an oven temperature  $T_{\text{oven}} = 365$  °C (activation I, Table 1), the  
16 catalysts react differently. Maximum temperatures for Co/Fe, Fe|MgO (not shown) and Co|SiO<sub>2</sub> vary  
17 between 353 and 360 °C (Fig. 5, A), while Fe/Mn|MgO shows a maximum temperature of 369 °C exceeding  
18 the oven temperature. This indicates the production of heat, which might results from significant amounts of  
19 precursor materials (metal nitrates) that were not fully oxidized during calcination. No exothermic behavior  
20 during activation with CO is observed (Fig. 5, B).

21 During synthesis experiments, Fe|MgO, Fe/Mn|MgO and Co|SiO<sub>2</sub> do not release significant amounts of heat.

22 This is exemplified in Fig. 5 (C) for Fe/Mn|MgO at different oven temperatures. The form of the temperature

1 distribution inside of the fixed bed follows a Gaussian function, while the temperatures at both ends of the  
 2 bed are nearly linearly dependent on the oven temperature. This indicates that the temperature distribution is  
 3 mostly caused by the oven. Since the loading of the active component Fe or Co is low (Table 2) for the  
 4 supported catalysts, this behavior is expected at low GHSV values.

5 A significant heat release is expected for the bulk catalysts especially at the front of the fixed bed. This is  
 6 demonstrated for the Co/Fe catalyst in Fig. 5 (D). Between 330 and 400 °C, the temperature gradient is  
 7 comparably low and the form of the distribution is different relative to higher temperatures. A significant  
 8 amount of heat seems to be released in the first half of the fixed bed. At higher temperatures, the form of the  
 9 distribution is comparable to that in Fig. 3 (C), indicating that it is mostly caused by the oven.

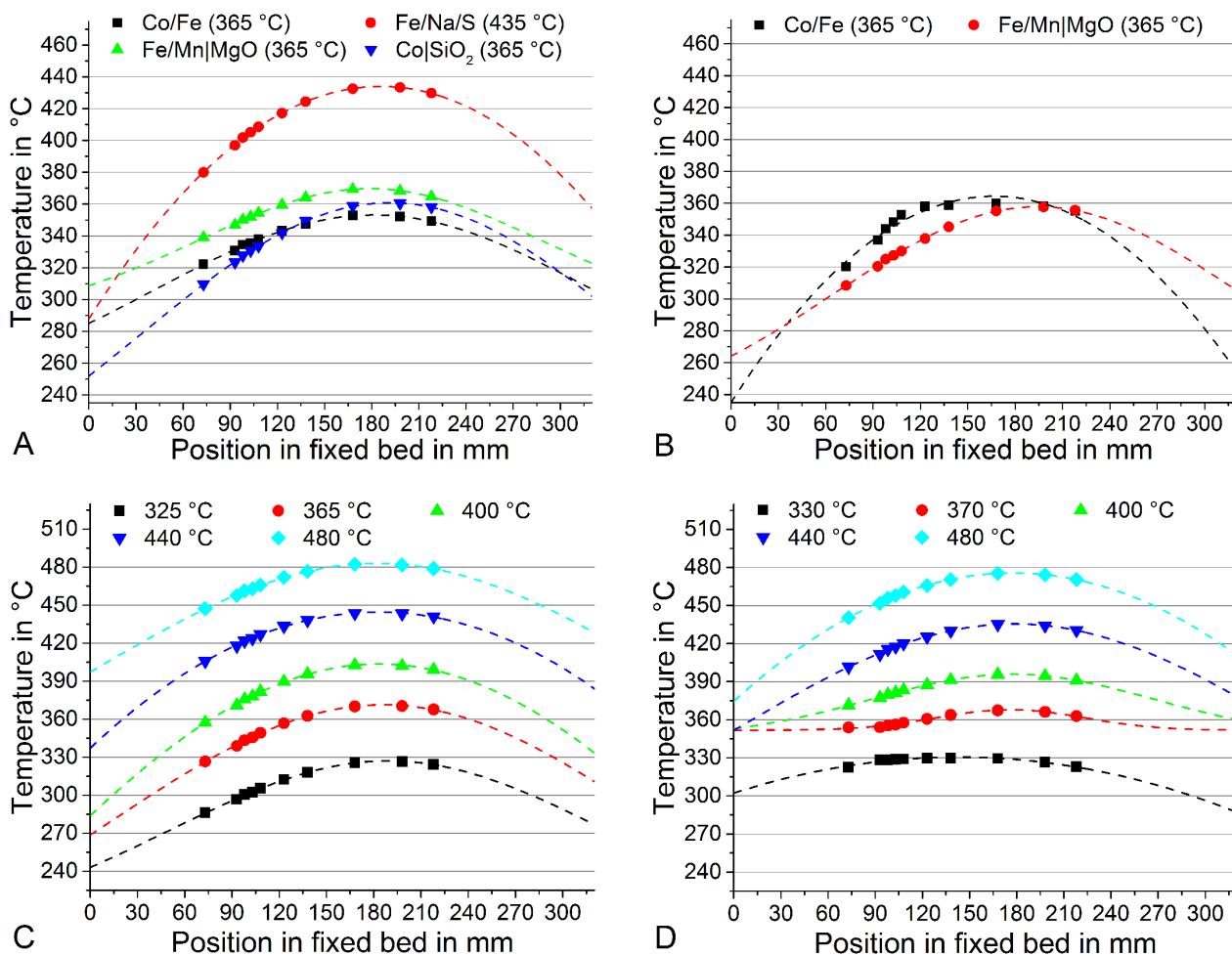


Fig. 5: Temperature distribution inside of the fixed bed during activation with H<sub>2</sub> (A, activation I) or CO (B, activation II for Fe/Mn|MgO and III for Co/Fe) and during synthesis after H<sub>2</sub> activation at different oven temperatures with Fe/Mn|

MgO (C) and Co/Fe (D). Solid lines represent the approximated temperature distribution with the help of a Gauß function.

Due to the high temperature gradients observed inside of the fixed bed during activation, different reduction levels of the active components are present. This follows from Table 4 and Table 5, which show the peak temperatures of the different reduction steps occurring during activation. Especially the fixed beds activated with H<sub>2</sub> contain significant amounts of iron or cobalt oxides since higher reduction temperatures are necessary with H<sub>2</sub> than with CO. Fe<sub>2</sub>O<sub>3</sub> and to a smaller extent also CoO are active catalysts for the water-gas shift reaction [31].

As a consequence, additional catalyst activation is likely to have taken place during synthesis studies at temperatures significantly higher than the activation temperature. Higher conversions of CO (and partly of H<sub>2</sub>), higher CO<sub>2</sub> selectivities and lower hydrocarbon selectivities would be observed at temperatures > 370 °C if additional catalyst activations take place. This might be the case with Fe|MgO, Fe/Mn|MgO, Co/Fe and Co|SiO<sub>2</sub> activated at an oven temperature of 365 °C. Nevertheless, the conclusions of this work concerning ethene selectivities are unaffected.

### 1 5.3 Conversion and selectivity at synthesis temperatures of 230 – 500 °C

2 Many data points have been collected and will be presented in diagrams in the following. Their description is  
 3 reduced to a minimum and apply to an H<sub>2</sub>/CO ratio of 3. In order to allow the fast recognition and  
 4 comparison of CO conversion and selectivities to C<sub>2</sub>H<sub>4</sub> and C<sub>2</sub>H<sub>6</sub>, these quantities are classified for each test  
 5 material as demonstrated in Table 6.

6

7 Table 6: Categories for the classification of CO conversion  $X_{CO}$  and selectivities  $S$  to C<sub>2</sub>H<sub>4</sub> and C<sub>2</sub>H<sub>6</sub>

	+	++	+++	++++	+++++
$X_{CO}$	< 2.5	2.5 – 25 %	25.1 – 50 %	50.1 – 75 %	> 75 %
$S_{C_2H_4}, S_{C_2H_6}$	< 0.3	0.3 – 3 %	3.1 – 6 %	6.1 – 9 %	> 9 %

8

#### 9 5.3.1 Fe|MgO

10 Table 7: CO conversion ( $X_{CO}$ ) and product selectivities ( $S_i$ ) to C<sub>2</sub>H<sub>4</sub> and C<sub>2</sub>H<sub>6</sub> at 350 and 450 °C for the Fe|MgO test  
 11 material at different activation conditions.

Activation conditions	$T_{max}$ in °C	$X_{CO}$	$S_{C_2H_4}$	$S_{C_2H_6}$
CO, 350 °C	350	++	+	+++
	450	+++++	+	+++++
H <sub>2</sub> , 350 °C	350	++	+	+
	450	+++++	+	+

12

1 No C<sub>2</sub>H<sub>4</sub> but C<sub>2</sub>H<sub>6</sub> is detected with this test material. C<sub>2</sub>H<sub>6</sub> selectivities peak at around 390 – 420 °C with  
 2 values of up to 12 % (Fig. 6). The catalytic performance is better with CO activation than with H<sub>2</sub> activation.  
 3 CH<sub>4</sub> and CO<sub>2</sub> are the main products generated at comparable amounts with H<sub>2</sub>/CO = 3, while CO<sub>2</sub>  
 4 concentrations are strongly increased with H<sub>2</sub>/CO = 1. The test material activated with H<sub>2</sub> shows a high CO<sub>2</sub>  
 5 selectivity (> 70 %) at T < 400 °C also in the case of H<sub>2</sub>/CO = 3. CO is effectively converted in all cases at T  
 6 > 430 °C, while H<sub>2</sub> conversion keeps < 40 %. H<sub>2</sub> conversion and CH<sub>4</sub> selectivity are higher than 40 % at T >  
 7 435 °C for the test material activated with H<sub>2</sub> since the reactor pressure increased from 1.7 up to 6.3 bar due  
 8 to the formation of carbonaceous depositions.

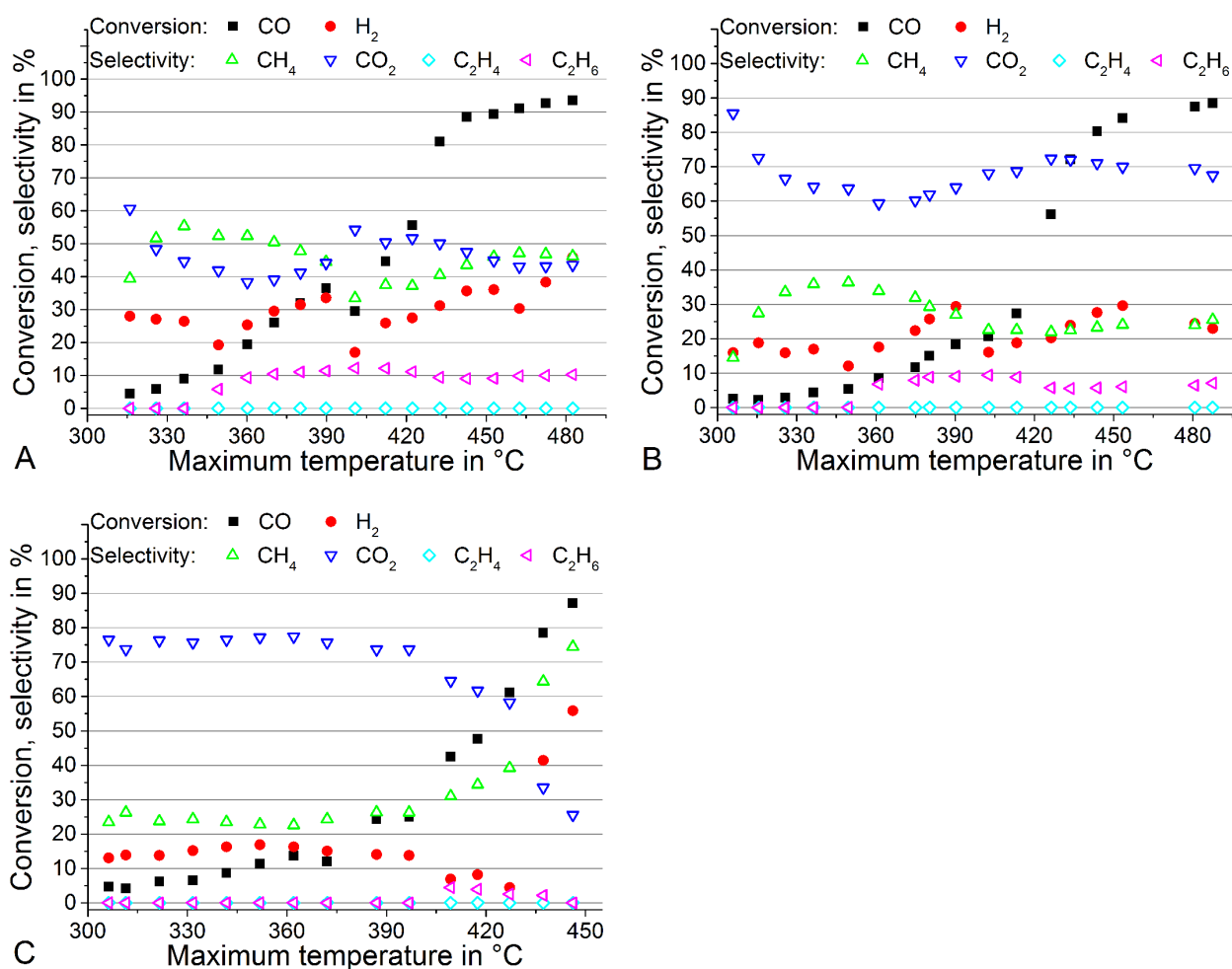


Fig. 6: Conversion and selectivity for the Fe|MgO test material after CO activation (activation II) at H<sub>2</sub>/CO = 3 (synthesis I: A) or H<sub>2</sub>/CO = 1 (synthesis II: B) and after H<sub>2</sub> activation (activation I) at H<sub>2</sub>/CO = 3 (synthesis I: C). For case C, an increased reactor pressure (up to 6.3 bar) at T > 420 °C likely causes the improved H<sub>2</sub> conversion and CH<sub>4</sub> selectivity.

### 1 5.3.2 Fe/Mn|MgO

2 Table 8: CO conversion ( $X_{\text{CO}}$ ) and selectivities ( $S_i$ ) to  $\text{C}_2\text{H}_4$  and  $\text{C}_2\text{H}_6$  at 350 and 450 °C for the Fe/Mn|MgO test material  
3 at different activation conditions.

Activation conditions	$T_{\text{max}}$ in °C	$X_{\text{CO}}$	$S_{\text{C}_2\text{H}_4}$	$S_{\text{C}_2\text{H}_6}$
CO, 350 °C	350	++	+	+
	450	++++	+++	+++++
H <sub>2</sub> , 350 °C	350	++	+	+
	450	+++	++++	+++++
H <sub>2</sub> , 420 °C	350	++	+	+
	450	++	+++++	+++

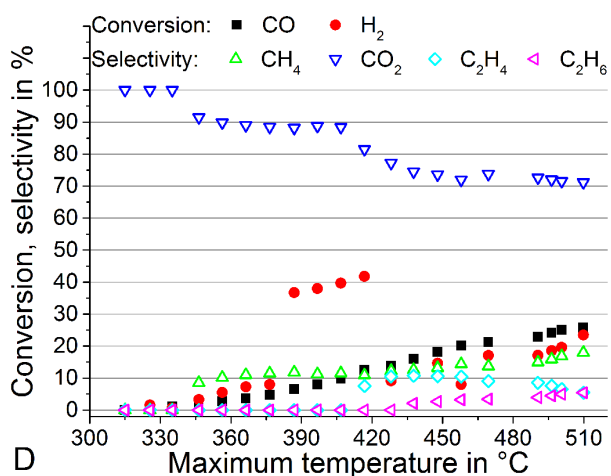
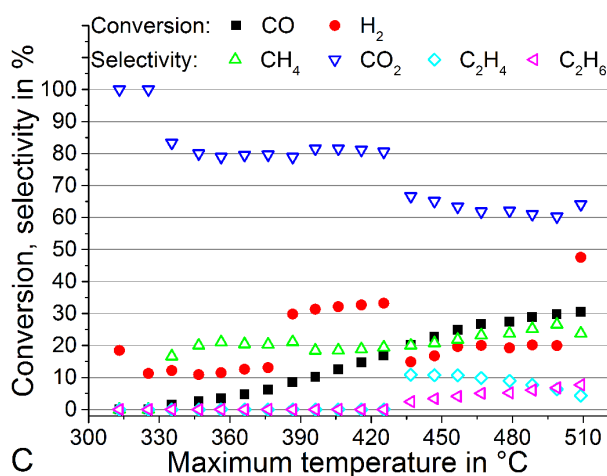
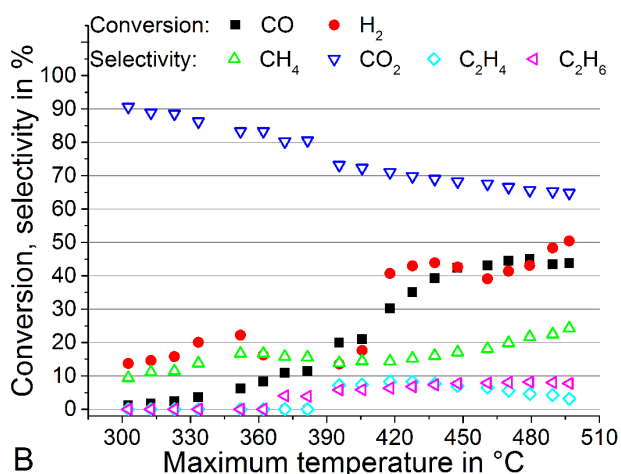
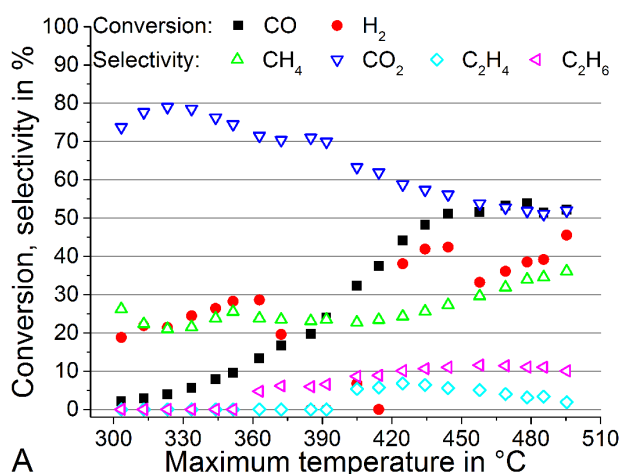
4  
5 Fe/Mn|MgO shows a lower activity than Fe|MgO considering the CO conversion (Fig. 7). CO conversion  
6 increases with temperature and reaches values up to 54 %, when the catalyst is activated with CO (Fig. 7, A,  
7 B). CO conversion does not exceed 32 %, when the catalyst is activated with H<sub>2</sub> (Fig. 7, C – E). No  
8 significant difference in CO conversion is observed for H<sub>2</sub> activation at 365 and 435 °C (Fig. 6, C, E).

9 Fe/Mn|MgO shows higher selectivities to CO<sub>2</sub> of > 70 % at  $T < 400$  °C and lower selectivities to CH<sub>4</sub> relative  
10 to Fe|MgO. The highest selectivities to C<sub>2</sub>H<sub>4</sub> of up to 11 % are observed for activation with H<sub>2</sub> at 420 °C at  
11 both H<sub>2</sub>/CO ratios of 3 and 1 (Fig. 7, C, D) in the temperature range of 425 – 460 °C. Selectivities to C<sub>2</sub>H<sub>6</sub>  
12 are below 4 % in these cases. In contrast, Fe/Mn|MgO activated with CO shows C<sub>2</sub>H<sub>4</sub> selectivity peaks at 410  
13 – 435 °C with values of up to 8 % (Fig. 7, A, B). C<sub>2</sub>H<sub>6</sub> selectivity peaks at 445 – 480 °C with values of up to  
14 11.5 %.

15 Activation with H<sub>2</sub> yields the highest selectivities to C<sub>2</sub>H<sub>4</sub> while C<sub>2</sub>H<sub>6</sub> is suppressed in this case. Variation of  
16 the activation temperature between 350 and 420 °C with H<sub>2</sub> has little influence. Activation with CO leads to  
17 higher C<sub>2</sub>H<sub>6</sub> selectivities at the expense of selectivity to C<sub>2</sub>H<sub>4</sub>. This is correlated to higher CO conversions  
18 observed for the CO-activated test material, which typically reduce the selectivity to unsaturated products  
19 [32,33]. This is discussed in more detail in section Selectivity to ethene.

20 [A full analysis of the product spectrum \(1 – 44 carbon atoms, quantification of alkanes, alkenes, alcohols,  
21 aldehydes and carboxylic acids\) was conducted by another research group and the method described in \[34\].](#)

1 The test material was activated with H<sub>2</sub> at 420 °C and the synthesis was conducted at 440 °C and H<sub>2</sub>/CO = 3  
 2 for ca. 100 h. After 80 h time on stream, the containers for different liquid and solid products were drained.  
 3 The product spectrum after full activation and carbide formation could be observed in this way (Fig. 7, F).  
 4 CO conversion amounted to 43.4 %, while the selectivities obtained are shown in Fig. 7 (F). The selectivity  
 5 values obtained are between those of Fig. 7, A and C, which shows that comparable conversions and  
 6 selectivities can be obtained with H<sub>2</sub> activation relative to CO activation but a longer time on stream is  
 7 necessary. Nearly twice as much C<sub>2</sub> – C<sub>4</sub> alkenes as C<sub>2</sub> – C<sub>4</sub> alkanes are formed and C<sub>5+</sub> products are minimal.  
 8 A significant amount of primarily built C<sub>2</sub>H<sub>4</sub> was likely converted into C<sub>2</sub>H<sub>6</sub> and C<sub>3</sub>H<sub>6</sub>. Besides alkenes and  
 9 alkanes, only very low selectivities to alcohols, aldehydes and carboxylic acids (named ‘remaining’ in Fig. 7,  
 10 F) are observed.



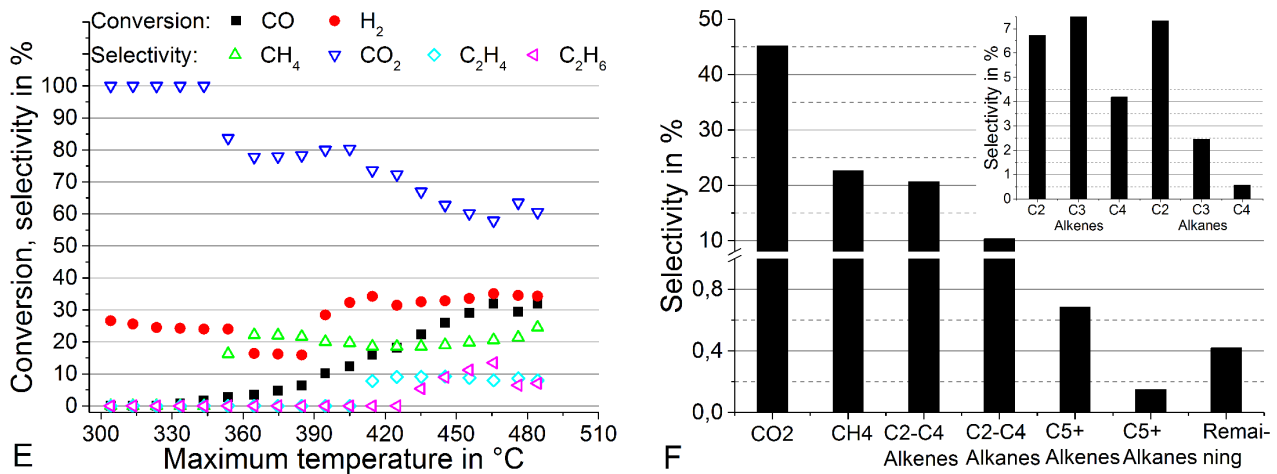


Fig. 7: Conversion and selectivity for the Fe/Mn/MgO test material. A – B: CO activation (activation II), synthesis with  $H_2/CO = 3$  (synthesis I: A) or  $H_2/CO = 1$  (synthesis II: B); C – D: H<sub>2</sub> activation (activation V), synthesis with  $H_2/CO = 3$  (synthesis I: C) or  $H_2/CO = 1$  (synthesis II: D); E: H<sub>2</sub> activation (activation I), synthesis with  $H_2/CO = 3$  (synthesis I); F: Full selectivity profile with H<sub>2</sub> activation (activation V) and synthesis at 440 °C with  $H_2/CO = 3$  after > 80 h time on stream. CO conversion amounted to 43.4 %.

### 5.3.3 Co|SiO<sub>2</sub>

Table 9: CO conversion ( $X_{CO}$ ) and selectivities ( $S_i$ ) to C<sub>2</sub>H<sub>4</sub> and C<sub>2</sub>H<sub>6</sub> at 350 and 450 °C for the Co|SiO<sub>2</sub> test material after H<sub>2</sub> activation.

Activation conditions	$T_{max}$ in °C	$X_{CO}$	$S_{C_2H_4}$	$S_{C_2H_6}$
H <sub>2</sub> , 350 °C	350	+++	+	++++
	450	+++++	+	+++

Co|SiO<sub>2</sub> shows comparable conversions of CO and H<sub>2</sub> at  $T < 370$  °C, while CO conversion increases stronger than H<sub>2</sub> conversion at higher temperatures (Fig. 8). A high selectivity to CH<sub>4</sub> of 56 – 70 % and CO<sub>2</sub> selectivities of 30 – 38 % are observed. C<sub>2</sub>H<sub>6</sub> is the only C<sub>2</sub> product detected and reaches selectivity values of up to 9.5 % at 345 °C. The selectivity to C<sub>2</sub>H<sub>6</sub> stays  $\geq 7$  % in the whole temperature range of 290 – 390 °C.

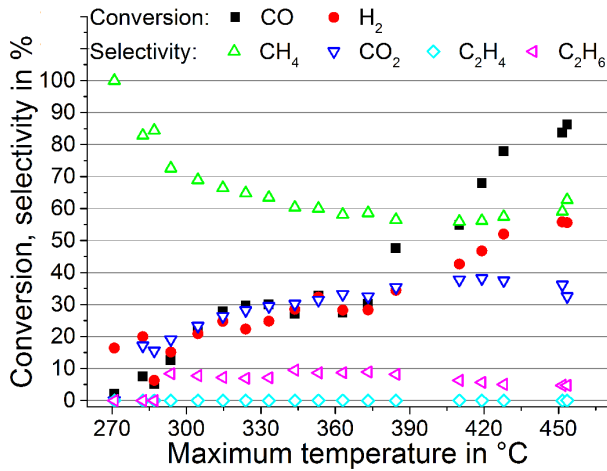


Fig. 8: Conversion and selectivity for the Co/SiO<sub>2</sub> test material after H<sub>2</sub> activation (activation I) and synthesis at H<sub>2</sub>/CO = 3 (synthesis I)

1

### 2 5.3.4 Co/Fe

3 Table 10: CO conversion ( $X_{CO}$ ) and selectivities ( $S_i$ ) to C<sub>2</sub>H<sub>4</sub> and C<sub>2</sub>H<sub>6</sub> at 350, 400 and 450 °C for the Co/Fe test material  
 4 after CO or H<sub>2</sub> activation.

Activation conditions	$T_{max}$ in °C	$X_{CO}$	$S_{C_2H_4}$	$S_{C_2H_6}$
CO, 350 °C	350	+++++	+	+++++
	450	+++++	+	++++
H <sub>2</sub> , 350 °C	350	+++++	+	+++
	400	+++++	+	++++

5

6 Activation and synthesis of the Co/Fe test material are always conducted with ca. 17 vol% of steam in order  
 7 to suppress the formation of coke, which starts already at temperatures of 300 – 320 °C with dry educt gas.  
 8 This catalyst shows a high activity considering CO conversions of > 90 % at  $T \geq 350$  °C (Fig. 9). Co/Fe  
 9 activated with CO shows CO conversions > 98.5 % in the whole temperature range (Fig. 9: A).

10 Selectivities to CO<sub>2</sub> and CH<sub>4</sub> typically vary between 17 and 30 % respectively 58 and 77 % for the CO-  
 11 activated material (Fig. 9: A). C<sub>2</sub>H<sub>6</sub> is the only C<sub>2</sub> product detected and has its highest selectivity of 12 % at  
 12 the lowest temperature studied (324 °C). High selectivities to CO<sub>2</sub> with values of 52 – 71 % are observed for  
 13 the H<sub>2</sub>-activated material at  $T < 350$  °C. Selectivities to CH<sub>4</sub> and C<sub>2</sub>H<sub>6</sub> amount to 22 – 38 % respectively 5 –  
 14 17 % (Fig. 9: B).

- 1 A low but steady pressure increase is observed at  $T > 370$  °C. This leads to a final absolute pressure of 2.3
- 2 bar for the CO-activated material and of  $> 6$  bar for the H<sub>2</sub>-activated material at the highest temperatures
- 3 studied (455 °C respectively 400 °C).

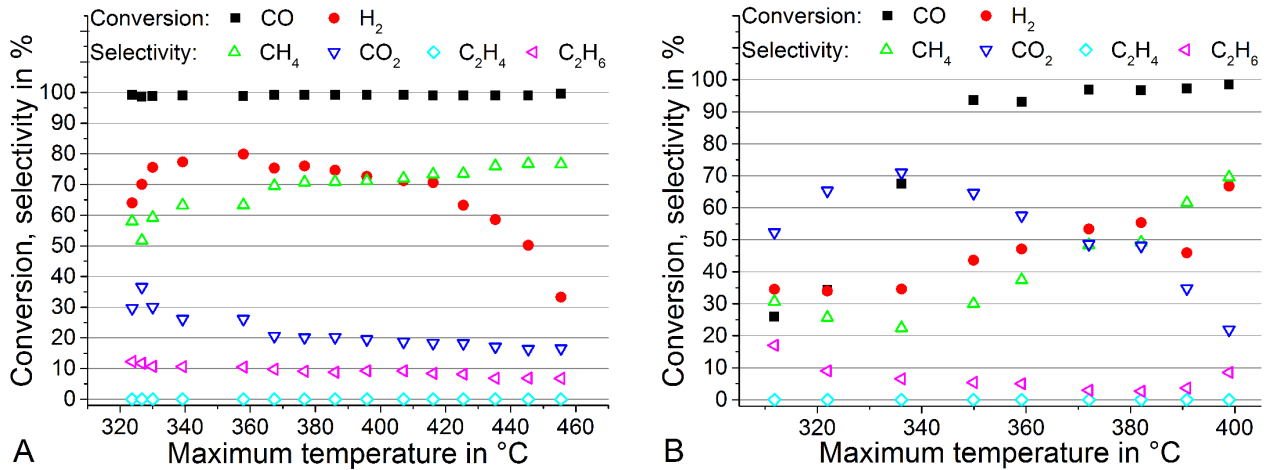


Fig. 9: Conversion and selectivity for the Co/Fe test material after CO activation (activation IV: A) and after H<sub>2</sub> activation (activation III: B) during synthesis at H<sub>2</sub>/CO = 3 (synthesis III).

- 4
- 5
- 6

### 7 5.3.5 Fe/Na/S

- 8 Table 11: CO conversion ( $X_{CO}$ ) and selectivities ( $S_i$ ) to C<sub>2</sub>H<sub>4</sub> and C<sub>2</sub>H<sub>6</sub> at 350 and 450 °C for the Fe/Mn|MgO test
- 9 material after H<sub>2</sub> activation.

Activation conditions	$T_{max}$ in °C	$X_{CO}$	$S_{C_2H_4}$	$S_{C_2H_6}$
H <sub>2</sub> , 350 °C	250	++++	+	+++++
	300	++++	+++	+++++
	350	+++++	+	+++++

10

- 11 No steam is added for Fe/Na/S, which leads to coke formation at  $T > 350$  °C. This test material is relatively
- 12 active at  $T > 250$  °C as indicated by a CO conversion value of  $> 60$  % at H<sub>2</sub>/CO = 3 in Fig. 10 (A). CO
- 13 conversion is significantly lower at H<sub>2</sub>/CO = 1 (Fig. 10, B). The conversion of H<sub>2</sub> does not exceed a value of
- 14 36 % ( $T < 350$  °C) and is between 20 and 30 % in the temperature range of 270 – 330 °C.

1 CO<sub>2</sub> is the main product with selectivities between 43 and 89 % (Fig. 10). CH<sub>4</sub> shows selectivities between 7  
 2 and 46 %. C<sub>2</sub>H<sub>4</sub> and C<sub>2</sub>H<sub>6</sub> are produced with maximum selectivities of 4.6 and 15.7 % at H<sub>2</sub>/CO = 3 as well  
 3 as of 7.2 and 8.5 % at H<sub>2</sub>/CO = 1. Maximum selectivities to C<sub>2</sub>H<sub>4</sub> and C<sub>2</sub>H<sub>6</sub> are observed in the temperature  
 4 ranges of 295 – 330 °C respectively 250 – 280 °C.

5 A test material containing only Fe and S shows comparable selectivities as Fe/Na/S, while its activity is  
 6 significantly lower. CO conversion reaches values of < 35 % at  $T < 350$  °C, while Fe/Na/S reaches values up  
 7 to 91 %.

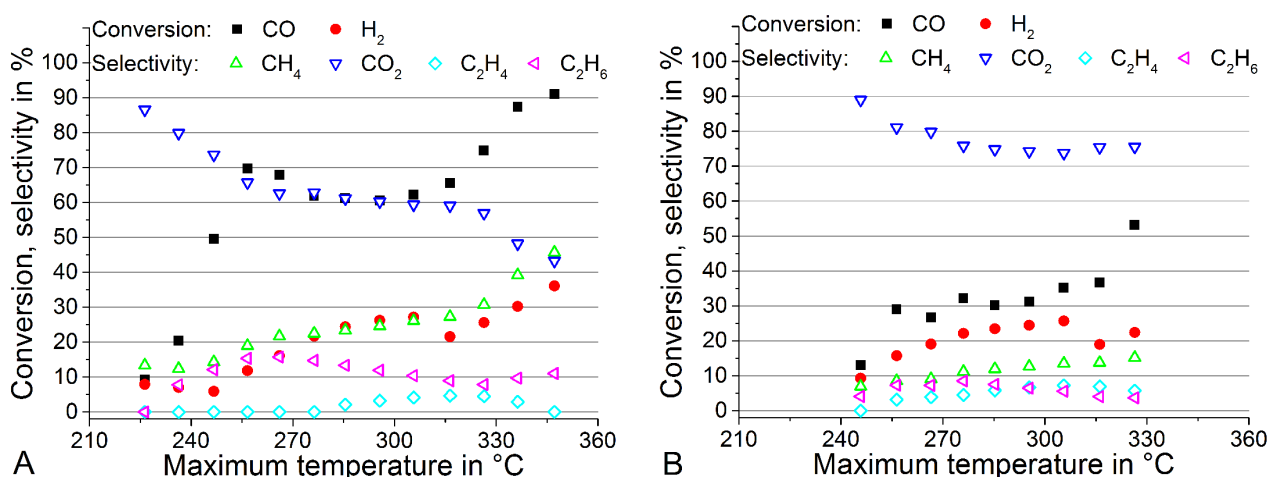


Fig. 10: Conversion and selectivity for the Fe/Na/S test material after H<sub>2</sub> activation (activation V) during synthesis at H<sub>2</sub>/CO = 3 (synthesis I: A) and H<sub>2</sub>/CO = 1 (synthesis II: B).

#### 8 5.4 Reactor pressure increase due to the formation of carbonaceous species

9 Increasing pressures at the reactor inlet are observed for each test material at a specific temperature  $T > 350$   
 10 °C. If the active material is supported, this temperature can be 50 K higher or more. Increased pressures  
 11 along the catalytic fixed bed originate from structural changes (swelling, fragmentation) and formation of  
 12 depositions [11,35,36], which increase the friction of the flowing gas. After passivation of used catalyst  
 13 samples, they can be observed visually. In most cases, force had to be used to remove the catalyst particles  
 14 from the reactor since a hard layer had formed in the reactor. While the supported catalyst particles are  
 15 darker after synthesis experiments, particles of bulk catalysts are “fused together” in a layer in the first third  
 16 of the reactor. This layer has to be broken during catalyst removal.

1 The resulting big particles (including  $\text{Al}_2\text{O}_3$  spheres of 2 – 3 mm size for bed dilution applied in earlier  
 2 experiments) and the original calcined particles for Co/Fe are displayed in Fig. 11. It appears that the  
 3 depositions formed fill the whole empty space between catalyst particles in the “fused region” so that the gas  
 4 could hardly pass the fixed bed.

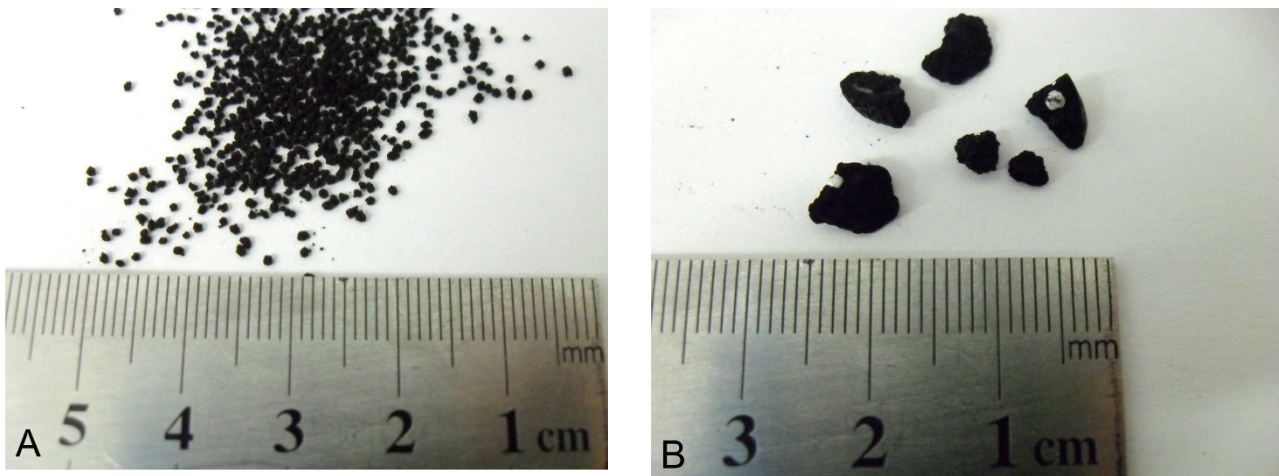


Fig. 11: Pictures of the calcined Co/Fe test material with particle diameters between 0.5 and 1 mm (A) and some fragments of the used fixed bed after synthesis at 350 °C without steam addition (diluted by alumina spheres) (B).

5  
 6 Fresh and used Co/Fe particles are heated in an oven with synthetic air passing by (temperature-programmed  
 7 oxidation, TPO), while the sample mass is measured. The related mass-loss diagram is shown in Fig. 12.  
 8 While the fresh particles lost only 5 % of the initial mass by heating up to 900 °C, the used sample lost about  
 9 55 %. The high mass loss of the used sample indicates that it consisted to about 50 % of a material, which  
 10 reacts with air and builds gaseous species or evaporates by heating.

11 Three major mass-loss areas appear at about 150 – 250, 300 – 370, and around 490 °C and are likely related  
 12 to different species. Temperature-programmed surface-reaction experiments with  $\text{H}_2$  instead of air are  
 13 described in the literature, which give a hint concerning the species formed [37,38]. Atomic carbon,  
 14 polymeric carbon, graphitic carbon and carbides are typical species present on used Co catalysts reacting  
 15 with  $\text{H}_2$  at different temperatures [37,38]. Based on these findings, the following assignment is suggested:  
 16 atomic carbon and carbides react with air at 150 – 250 °C, polymeric carbon at 300 – 370 °C and graphitic  
 17 carbon at around 490 °C. Following this assignment, polymeric carbon is the mostly formed carbonaceous  
 18 species on the Co/Fe catalyst.

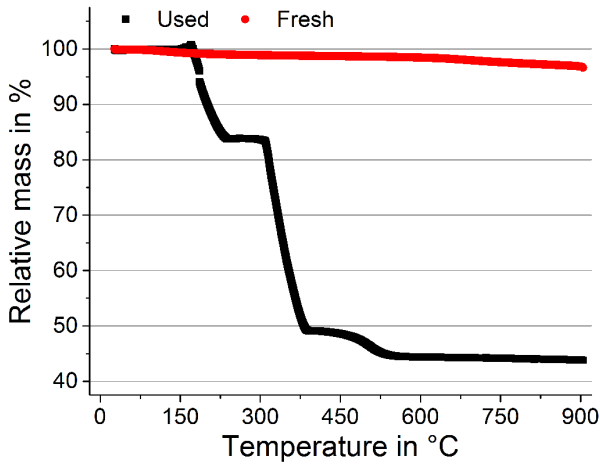


Fig. 12: Relative mass of fresh and used Co/Fe catalyst particles during TPO in synthetic air.

## 1 6 Discussion of the results

### 2 6.1 Estimation of C<sub>3</sub>, C<sub>4</sub> and C<sub>5+</sub> hydrocarbons

3 In Fischer-Tropsch synthesis, the distribution of linear hydrocarbons can be described by the ideal Anderson-  
 4 Schulz-Flory (ASF) distribution [39–41], displayed in Fig. 13 (A) for C<sub>1</sub> - C<sub>5+</sub> species. The ASF distribution  
 5 states that the molar fraction of hydrocarbons with  $N_C$  carbon atoms follows Eq. 7 and implies that the value  
 6 of  $\alpha$  is not dependent on the carbon number. Though deviations from the ideal ASF distribution exist in  
 7 several practical applications [33,42,43], it is applied in the following to estimate the mass fraction of C<sub>3</sub>, C<sub>4</sub>  
 8 and C<sub>5+</sub> hydrocarbons produced together with CH<sub>4</sub>, C<sub>2</sub>H<sub>4</sub> and C<sub>2</sub>H<sub>6</sub>.

Eq. 7

Eq. 8

9 It follows from Eq. 7 that the ratio of products with carbon number two and one is equivalent to the chain  
 10 growth probability  $\alpha$  (Eq. 8). Its dependence on maximum reactor temperature, catalyst, activation agent and  
 11 H<sub>2</sub>/CO ratio is displayed in Fig. 13 (B, C).

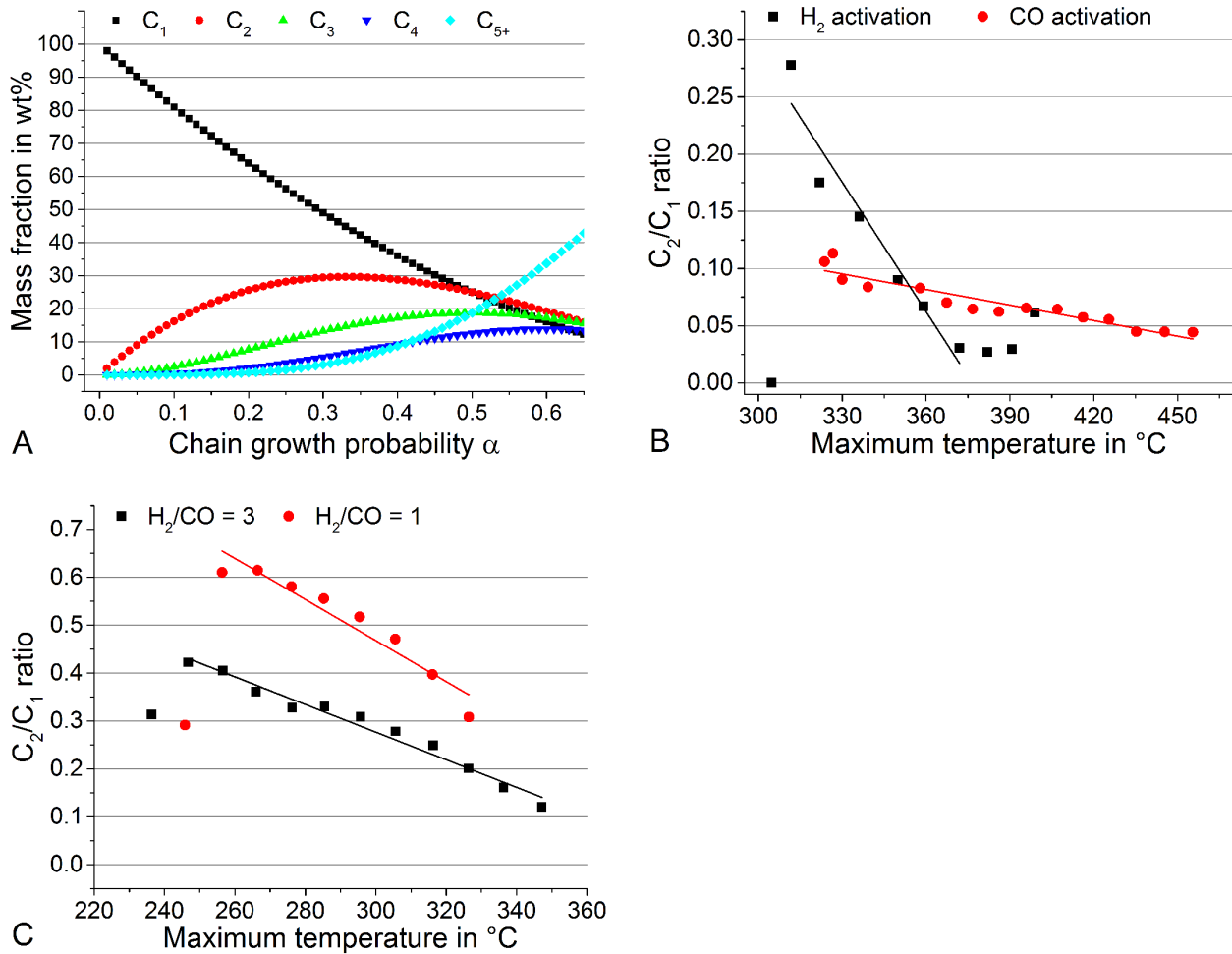


Fig. 13: A: Ideal Anderson-Schulz-Flory distribution for  $C_1$ ,  $C_2$ ,  $C_3$ ,  $C_4$  and  $C_{5+}$  hydrocarbons produced in Fischer-Tropsch synthesis in dependence of the chain growth probability  $\alpha$ . B – C: Ratio of  $C_2$  and  $C_1$  products (equivalent to the chain growth probability  $\alpha$ ) received with Co/Fe (after  $\text{H}_2$  and CO activation at  $350\text{ }^{\circ}\text{C}$ , synthesis at  $\text{H}_2/\text{CO} = 3$ : B) and Fe/Na/S (after  $\text{H}_2$  activation at  $420\text{ }^{\circ}\text{C}$ : C).

- 1 Maximum amounts of  $C_2 - C_4$  hydrocarbons at low  $C_{5+}$  fractions ( $< 20\text{ wt}\%$ ) are received at  $\alpha$  values
- 2 between 0.3 and 0.5 (Fig. 13, A). The Co/Fe test material shows low  $C_2/C_1$  ratios of 0.04 – 0.11 after CO
- 3 activation and of 0.03 – 0.28 after  $\text{H}_2$  activation (Fig. 13, B).  $C_2/C_1$  ratio values for Fe/Na/S are significantly
- 4 higher and vary between 0.12 and 0.42 at  $\text{H}_2/\text{CO} = 3$  and between 0.31 and 0.61 at  $\text{H}_2/\text{CO} = 1$  (Fig. 13, C). A
- 5 decreasing  $C_2/C_1$  ratio with increasing reactor temperature is expected since the probability for chain growth
- 6 is higher at low temperatures than at high temperatures [33].
- 7 For comparison,  $\alpha$  values received by other authors are reported.  $\text{Fe}_2\text{O}_3$  and a commercial Fe/Cu/K catalyst
- 8 from Ruhrchemie show values of 0.57 at  $240\text{ }^{\circ}\text{C}$  and of 0.24 at  $320\text{ }^{\circ}\text{C}$  at  $\text{H}_2/\text{CO} = 3$  and reactor pressures
- 9 between 8 and 20 bar [33,44,45]. These values are close to the  $\alpha$  values observed for Fe/Na/S at  $\text{H}_2/\text{CO} = 3$

1 and pressures of < 1.5 bar (Fig. 13, C). The temperature range for high fractions of C<sub>2</sub> – C<sub>4</sub> hydrocarbons is  
2 between 240 and 340 °C for Fe/Na/S at H<sub>2</sub>/CO ratios between 1 and 3.

### 3 6.2 Selectivity to ethene

4 With the test materials Fe/Mn|MgO, Fe/Na/S and Fe/S, selectivities to ethene of up to 11 % are observed,  
5 while no ethene is detected with the other materials. Nevertheless, ethane is found with every test material  
6 with selectivities of up to 17 %. Table 12 summarises CO conversion and selectivities to CH<sub>4</sub>, CO<sub>2</sub>, C<sub>2</sub>H<sub>4</sub> and  
7 C<sub>2</sub>H<sub>6</sub> for every test material at the synthesis conditions with the highest selectivities to ethene or, if no ethene  
8 is detected, to ethane.

9 The highest selectivities to ethene are observed at low and medium conversions of CO between 18 and 44 %  
10 (Table 12). This observation can be explained by the fact that ethene and other light alkenes are likely  
11 readsorbed on the catalyst surface and participate in secondary reactions (isomerization, hydrogenation)  
12 [26,33,46,47]. Secondary reactions can be inhibited if the CO partial pressure is high due to competitive  
13 adsorption of CO and alkenes for the same catalytic sites [33]. At high CO conversions, the CO partial  
14 pressure is low in the rear half of a fixed bed so that alkenes can readsorb easily and undergo secondary  
15 reactions. This leads to lower alkene concentrations relative to the case when CO conversions are low.

16 High selectivities to ethene relative to ethane at low GHSV values are a clear effect of catalyst promoters.  
17 This follows from the comparison between Fe|MgO and Fe/Mn|MgO (Table 12). With Fe/Mn|MgO,  
18 maximum selectivities to ethene reach values between 7 and 11 %, while no ethene is found with Fe|MgO.  
19 Xu et al. explain this finding with the ability of manganese to block hydrogenation sites on the catalyst  
20 surface [26]. A comparable ability is expected from sulphur so that secondary reactions of light alkenes are  
21 less likely [24,48]. Promoters like sodium and potassium improve the ability of the catalyst to adsorb and  
22 convert CO so that CO conversions are higher with Na or K promoted materials relative to unpromoted ones  
23 at the same reaction conditions [26,48]. This is supported by comparison of the results for Fe/Na/S and Fe/S  
24 (section Fehler: Referenz nicht gefunden and Table 12).

- 1 Table 12: CO conversion  $X_{CO}$ , product selectivities  $S_i$ , product yields  $Y_i$  and  $C_2/C_1$  ratios for each test material at the  
 2 highest selectivity to ethene or, if no ethene is detected, to ethane during synthesis at a defined  $H_2/CO$  ratio and  
 3 maximum temperature  $T_{max}$  in the fixed bed

Test material	Reduction conditions	$T_{max}$ in °C	$H_2/CO$ ratio	$X_{CO}$	in %						
					$S_{CH_4}$	$S_{CO_2}$	$S_{C_2H_4}$	$S_{C_2H_6}$	$Y_{C_2H_4}$	$Y_{C_2H_6}$	$C_2/C_1$ ratio
Fe MgO	H <sub>2</sub> , 350 °C	409	3	42. 5	31.0	64. 5	0	4.4	0	1.9	0.07
	CO, 350 °C	401	3	29. 5	33.5	54. 3	0	12.2	0	3.6	0.18
	CO, 350 °C	403	1	20. 7	22.5	68. 1	0	9.4	0	1.9	0.21
Fe/Mn MgO	H <sub>2</sub> , 420 °C	437	3	20. 2	20.0	66. 7	10.9	2.5	2.2	0.5	0.33
	H <sub>2</sub> , 420 °C	448	1	18. 1	13.2	73. 6	10.6	2.6	1.9	0.5	0.50
	H <sub>2</sub> , 350 °C	446	3	26. 1	19.1	62. 8	9.2	9.0	2.4	2.3	0.48
	CO, 350 °C	425	3	44. 1	24.3	58. 8	6.8	10.1	3.0	4.5	0.35
	CO, 350 °C	428	1	35. 0	15.2	69. 8	8.2	6.8	2.9	2.4	0.49
Co/Fe	H <sub>2</sub> , 350 °C	312	3	25. 9	30.6	52. 3	0	17.0	0	4.4	0.28
	CO, 350 °C	324	3	99. 3	58.0	29. 7	0	12.3	0	12.2	0.11
Fe/Na/S	H <sub>2</sub> , 420 °C	316	3	65. 6	27.3	59. 7	4.6	13.6	3.0	8.9	0.25
	H <sub>2</sub> , 420 °C	306	1	35. 2	13.5	73. 7	7.2	12.7	2.5	4.5	0.47
Fe/S	H <sub>2</sub> , 420 °C	366	3	57. 4	26.6	58. 1	0	15.4	0	8.8	0.29
	H <sub>2</sub> , 420 °C	368	1	37. 3	15.6	70. 7	5.4	13.7	2.0	5.1	0.44
Co SiO <sub>2</sub>	H <sub>2</sub> , 350 °C	344	3	27. 1	60.3	30. 2	0	9.5	0	2.6	0.08

- 4  
 5 Another evaluation is done based on reaction velocities (Eq. 9 and Eq. 10). Eq. 9 is valid for the volume-  
 6 based reaction rate and takes the difference in the molar concentration of CO between inlet and outlet  $\Delta c_{CO}$   
 7 as well as the contact time of the gas with the catalyst  $\Delta t$  into account. Eq. 10 represents the reaction rate  
 8 based on the mass of iron and cobalt in each test material  $m_{Fe,Co}$ .  $f_{Fe,Co}$  represents the fraction of Fe and Co in a  
 9 test material in Eq. 10.  $\Delta t$  is equivalent to the quotient of the bed volume  $V_{bed}$  and the volumetric flow rate so  
 10 that the right formula of Eq. 10 can be applied with known values. The cases with the highest yields to  $C_2$

1 products from Table 12 are compared in Table 13 with the help of the mass-bases reaction rate (Eq. 10). The  
 2 reaction rate to C<sub>2</sub> products is quoted as well.

3 The order of reaction rates to C<sub>2</sub> products based on Fe and Co mass follows from Table 13: Fe/Mn|MgO >  
 4 Fe|MgO > Fe/Na/S > Fe/S > Co/Fe > Co|SiO<sub>2</sub>. The corresponding order of rates to ethene is Fe/Mn|MgO >  
 5 Fe/Na/S > Fe/S and supports the statements made in the first part of this section.

6 Table 13: Reaction rates for the cases of Table 12 with the highest yields to ethene or ethane based on bed volume ( $r_V$ )  
 7 and mass of Fe and Co in each test material ( $r_m$ ). The last column includes the selectivity to C<sub>2</sub> products ( $r_{m,CO \rightarrow C_2}$ ).

<u>Test material</u>	<u>Reduction conditions</u>	<u><math>T_{max}</math> in °C</u>	<u>H<sub>2</sub>/CO ratio</u>	<u><math>m_{bed}</math> in g</u>	<u><math>m_{Fe,Co}</math> in g</u>	<u><math>r_{V,CO}</math> in mmol m<sup>-3</sup> s<sup>-1</sup></u>	<u><math>r_{m,CO}</math> in mmol kg<sup>-1</sup> s<sup>-1</sup></u>	<u><math>r_{m,CO \rightarrow C_2}</math> in mmol kg<sup>-1</sup> s<sup>-1</sup></u>
<u>Fe MgO</u>	<u>CO, 350 °C</u>	<u>401</u>	<u>3</u>	<u>50.</u> <u>8</u>	<u>4.4</u>	<u>94.1</u>	<u>1.57</u>	<u>0.19</u>
<u>Fe/Mn MgO</u>	<u>CO, 350 °C</u>	<u>425</u>	<u>3</u>	<u>58.</u> <u>3</u>	<u>5.4</u>	<u>104.1</u>	<u>1.41</u>	<u>0.24</u>
<u>Co/Fe</u>	<u>CO, 350 °C</u>	<u>324</u>	<u>3</u>	<u>67.</u> <u>9</u>	<u>47.8</u>	<u>493.4</u>	<u>0.76</u>	<u>0.13</u>
<u>Fe/Na/S</u>	<u>H<sub>2</sub>, 420 °C</u>	<u>316</u>	<u>3</u>	<u>34.</u> <u>4</u>	<u>23.8</u>	<u>459.2</u>	<u>0.90</u>	<u>0.16</u>
<u>Fe/S</u>	<u>H<sub>2</sub>, 420 °C</u>	<u>368</u>	<u>1</u>	<u>56.</u> <u>3</u>	<u>39.0</u>	<u>392.3</u>	<u>0.74</u>	<u>0.14</u>
<u>Co SiO<sub>2</sub></u>	<u>H<sub>2</sub>, 350 °C</u>	<u>344</u>	<u>3</u>	<u>40.</u> <u>3</u>	<u>8.1</u>	<u>34.0</u>	<u>0.31</u>	<u>0.03</u>

## 9 | 7 Summary and conclusions

10 Iron and cobalt containing test materials for the conversion of H<sub>2</sub> and CO into light hydrocarbons (alkenes as  
 11 target products) were studied. The high selectivities to light alkenes published [23–27] could not be  
 12 reproduced by this work. One reason for this is the low GHSV value of 160 h<sup>-1</sup> applied in this study, which  
 13 facilitates the conversion of primarily built alkenes (especially ethene) in secondary reactions. A second  
 14 reason are incomplete balances provided by individual references (e. g. no inclusion of CO<sub>2</sub>), which  
 15 overestimate the real selectivities to light alkenes. Besides, differences in the catalyst composition and the  
 16 application of an extended fixed bed with large temperature gradients are other reasons for the limited  
 17 reproducibility.

1 In the case of the Co/Fe catalyst of Mirzaei et al. [23], no alkene selectivity was found. C<sub>2</sub>H<sub>6</sub> was the only C<sub>2+</sub>  
2 product detected in this work though C<sub>2</sub>H<sub>4</sub> and C<sub>3</sub>H<sub>6</sub> were the major products in the study of Mirzaei et al.  
3 The low GHSV of 160 h<sup>-1</sup> applied in this work relative to 4000 – 5000 h<sup>-1</sup> used by Mirzaei et al. is the major  
4 difference, while the catalyst compositions were nearly identical. Our results confirm that the selectivity to  
5 light alkenes (especially ethene) is sensitive to GHSV and that light alkenes are converted totally at low  
6 GHSV<sup>2</sup>s and very high CO conversions.

7 In the case of Fe|MgO and Fe/Mn|MgO, modifications of the catalyst composition relative to the publications  
8 of Xu et al. were applied [25,26]. Fe on an MgO support did not produce alkenes (up to the detection limit).  
9 The addition of Mn to Fe|MgO strongly improved the ethene selectivity up to a value of 11 %, while the  
10 C<sub>2</sub>H<sub>6</sub> selectivity was reduced. At the same time, the selectivity to CO<sub>2</sub> was increased by the addition of Mn,  
11 which is a drawback of high Mn loadings. Nevertheless, Fe/Mn|MgO showed the highest selectivities to C<sub>2</sub>  
12 – C<sub>4</sub> alkenes at CO conversions of 40 – 50 % with low selectivities of < 0.5 % to alcohols, aldehydes and  
13 carboxylic acids.

14 The test material Fe/Na/S showed ethene selectivities of up to 7 %, while CO<sub>2</sub> and C<sub>2</sub>H<sub>6</sub> selectivities reached  
15 values of 74 and 13 %, respectively. The low GHSV applied also reduces the selectivities to alkenes in this  
16 case since higher values were reported by Botes et al. [24,47]. The comparison between Fe/S and Fe/Na/S  
17 confirms the beneficial effect of Na as promotor leading to higher CO conversions but also to higher CO<sub>2</sub>  
18 selectivities.

19 With Co|SiO<sub>2</sub>, C<sub>2</sub>H<sub>6</sub> was the only C<sub>2</sub> product detected and reached selectivity values of up to 9.5 % at 345 °C.  
20 CH<sub>4</sub> was the main product, while CO<sub>2</sub> selectivities were low (< 40 %) relative to Fe containing test materials.  
21 This is justified by the low water-gas shift activity of Co.

22 In order to produce light alkenes directly from syngas commercially, the following operational limitations  
23 are recommended by this study:

- 24 • GHSV > 300 h<sup>-1</sup>,
- 25 • T < 350 °C for bulk catalysts,

1 •  $T < 500 \text{ }^\circ\text{C}$  for supported catalysts,

2 | •  $1.5 < p < 10 \text{ bar}$  and

3 | •  $1 \leq \text{H}_2/\text{CO} \leq 3$ .

4 Besides these conditions, catalyst promoters like Mn or S for reduced losses of primary alkenes by secondary  
5 reactions and Na or K for increased CO conversions should be applied. The co-production of  $\text{CO}_2$  has to be  
6 limited as well, which can be realized by an optimization of GHSV and catalyst composition.

7 |

## 8 | Acknowledgement

9 The authors thank Eric Mattheß, Max Schaller and Dr. Erik Reichelt from the Fraunhofer Institute for  
10 Ceramic Technologies and Systems IKTS in Dresden, Germany, for conducting the catalytic measurements  
11 with the Fe/Mn|MgO test material depicted in Fig. 7 (F).

12 |

Abbreviation	Description
<u>ASF</u>	<u>Anderson-Schulz-Flory</u>
<u>FT</u>	<u>Fischer-Tropsch</u>
<u>GC-FID</u>	<u>Gas chromatograph with flame ionization detector</u>
<u>GC-MS</u>	<u>Gas chromatograph with mass spectrometer</u>
<u>GC-TDC</u>	<u>Gas chromatograph with thermal conductivity detector</u>
<u>GHSV</u>	<u>Gas hourly space velocity</u>
<u>MFC</u>	<u>Mass flow controller</u>
<u>XRF</u>	<u>X-ray fluorescence spectroscopy</u>
<u>XRF</u>	<u>X-ray fluorescence spectroscopy</u>
<u>GC-TDC</u>	<u>Gas chromatograph with thermal conductivity detector</u>
<u>GC-FID</u>	<u>Gas chromatograph with flame ionization detector</u>
<u>GC-MS</u>	<u>Gas chromatograph with mass spectrometer</u>
<u>GHSV</u>	<u>Gas hourly space velocity</u>
<u>MFC</u>	<u>Mass flow controller</u>
<u>FT</u>	<u>Fischer-Tropsch</u>
<u>ASF</u>	<u>Anderson-Schulz-Flory</u>

13 |

Symbol	Description	Unit
<u><math>\alpha</math></u>	<u>Chain growth probability</u>	<u>=</u>

$c$	<u>Molar concentration</u>	<u>mol m<sup>-3</sup></u>
$f_{\text{Fe,CO}}$	<u>Fraction of Fe and Co in a test material</u>	=
$g$	<u>Specific gas species: CO, CO<sub>2</sub>, CH<sub>4</sub>, C<sub>2</sub>H<sub>4</sub>, C<sub>2</sub>H<sub>6</sub></u>	=
$N_C$	<u>Number of carbon atoms in a species</u>	=
	<u>Molar flow rate</u>	<u>mol s<sup>-1</sup></u>
$p$	<u>Pressure</u>	<u>Pa</u>
$R$	<u>Universal gas constant</u>	<u>J K<sup>-1</sup> mol<sup>-1</sup></u>
	<u>Density of the fixed bed</u>	<u>kg m<sup>-3</sup></u>
$S$	<u>Product selectivity for CO<sub>2</sub>, CH<sub>4</sub>, C<sub>2</sub>H<sub>4</sub>, C<sub>2</sub>H<sub>6</sub> based on CO conversion</u>	<u>%</u>
$T$	<u>Absolute temperature</u>	<u>K</u>
	<u>Volumetric flow rate</u>	<u>m<sup>3</sup> s<sup>-1</sup></u>
$X$	<u>Educt conversion for CO and H<sub>2</sub></u>	<u>%</u>
$y$	<u>Volumetric concentration</u>	<u>vol%</u>
$Y$	<u>Product yield for C<sub>2</sub>H<sub>4</sub> and C<sub>2</sub>H<sub>6</sub> based on CO conversion</u>	<u>%</u>
$y^*$	<u>Molar fraction</u>	<u>mol%</u>
$y$	<u>Volumetric concentration</u>	<u>vol%</u>
$y^*$	<u>Molar fraction</u>	<u>mol%</u>
$g$	<u>Specific gas species: CO, CO<sub>2</sub>, CH<sub>4</sub>, C<sub>2</sub>H<sub>4</sub>, C<sub>2</sub>H<sub>6</sub></u>	
$X$	<u>Educt conversion for CO and H<sub>2</sub></u>	<u>%</u>
$Y$	<u>Product yield for C<sub>2</sub>H<sub>4</sub> and C<sub>2</sub>H<sub>6</sub> based on CO conversion</u>	<u>%</u>
$S$	<u>Product selectivity for CO<sub>2</sub>, CH<sub>4</sub>, C<sub>2</sub>H<sub>4</sub>, C<sub>2</sub>H<sub>6</sub> based on CO conversion</u>	<u>%</u>
	<u>Molar flow rate</u>	<u>mol s<sup>-1</sup></u>
$N_C$	<u>Number of carbon atoms in a species</u>	

1

## 2 References

- 3 [1] R. Guettel, U. Kunz, T. Turek, Reactors for Fischer-Tropsch Synthesis, Chem. Eng. Technol. 31 (5)  
4 (2008) 746–754.
- 5 [2] H. Schulz, Short history and present trends of Fischer–Tropsch synthesis, Applied Catalysis A: General  
6 186 (1-2) (1999) 3–12.
- 7 [3] B. Jager, R. Espinoza, Advances in low temperature Fischer-Tropsch synthesis, Catalysis Today 23 (1)  
8 (1995) 17–28.
- 9 [4] A. de Klerk, E. Furimsky, Catalysis in the Refining of Fischer-Tropsch Syncrude, Royal Society of  
10 Chemistry, Cambridge, 2010.
- 11 [5] E. Kemf (Ed.), GCO--Global Chemicals Outlook: Towards sound management of chemicals, United  
12 Nations Environment Programme, Nairobi, Kenya, 2013.

- 1 [6] R. Mülhaupt, *Green Polymer Chemistry and Bio-based Plastics: Dreams and Reality*, *Macromol. Chem.*  
2 *Phys.* 214 (2) (2013) 159–174.
- 3 [7] Institute for Bioplastics and Biocomposites, *Biopolymers: facts and statistics*, 2015.
- 4 [8] M.J. Gradassi, N. Wayne Green, *Economics of natural gas conversion processes*, *Fuel Processing*  
5 *Technology* 42 (2-3) (1995) 65–83.
- 6 [9] T. Ren, M. Patel, K. Blok, *Steam cracking and methane to olefins: Energy use, CO<sub>2</sub> emissions and*  
7 *production costs*, *Energy* (2008).
- 8 [10] P. Tian, Y. Wei, M. Ye, Z. Liu, *Methanol to Olefins (MTO): From Fundamentals to*  
9 *Commercialization*, *ACS Catal.* 5 (3) (2015) 1922–1938.
- 10 [11] H.M. Torres Galvis, K.P. de Jong, *Catalysts for Production of Lower Olefins from Synthesis Gas: A*  
11 *Review*, *ACS Catal.* 3 (9) (2013) 2130–2149.
- 12 [12] S. Aguado, G. Bergeret, C. Daniel, D. Farrusseng, *Absolute molecular sieve separation of*  
13 *ethylene/ethane mixtures with silver zeolite A*, *Journal of the American Chemical Society* 134 (36)  
14 (2012) 14635–14637.
- 15 [13] S.-H. Cho, J.-H. Park, S.-S. Han, J.-N. Kim, *Comparison of AgNO<sub>3</sub>/Clay and AgNO<sub>3</sub>/ALSG Sorbent*  
16 *for Ethylene Separation*, *Adsorption* 11 (S1) (2005) 145–149.
- 17 [14] P. Piermartini, P. Pfeifer, *Microreactor Approaches for Liquid Fuel Production from Bioderived Syngas*  
18 *–5 m<sup>3</sup>/h Prototype Development for HTHP Water Gas Shift*, *Ind. Eng. Chem. Res.* 54 (16) (2015)  
19 4561–4571.
- 20 [15] H. Zohdi-Fasaei, H. Atashi, F. Farshchi Tabrizi, A.A. Mirzaei, *Modeling and optimization of Fischer-*  
21 *Tropsch synthesis over Co-Mn-Ce/SiO<sub>2</sub> catalyst using hybrid RSM/LHHW approaches*, *Energy* 128  
22 (2017) 496–508.
- 23 [16] N. Lohitharn, J.G. Goodwin Jr., E. Lotero, *Fe-based Fischer–Tropsch synthesis catalysts containing*  
24 *carbide-forming transition metal promoters*, *Journal of Catalysis* 255 (1) (2008) 104–113.
- 25 [17] K. Sudsakorn, *Effect of activation method on Fe FTS catalysts: Investigation at the site level using*  
26 *SSITKA*, *Journal of Catalysis* 213 (2) (2003) 204–210.

- 1 [18] T. Herranz, S. Rojas, F. Perezalonso, M. Ojeda, P. Terreros, J. Fierro, Genesis of iron carbides and their  
2 role in the synthesis of hydrocarbons from synthesis gas, *Journal of Catalysis* 243 (1) (2006) 199–211.
- 3 [19] M.D. Shroff, D.S. Kalakkad, K.E. Coulter, S.D. Kohler, M.S. Harrington, N.B. Jackson, A.G. Sault,  
4 A.K. Datye, Activation of Precipitated Iron Fischer-Tropsch Synthesis Catalysts, *Journal of Catalysis*  
5 156 (2) (1995) 185–207.
- 6 [20] H. Schulz, Selforganization in Fischer–Tropsch synthesis with iron- and cobalt catalysts, *Catalysis*  
7 *Today* 228 (2014) 113–122.
- 8 [21] D.S. Kalakkad, M.D. Shroff, S. Köhler, N. Jackson, A.K. Datye, Attrition of precipitated iron Fischer-  
9 Tropsch catalysts, *Applied Catalysis A: General* 133 (2) (1995) 335–350.
- 10 [22] H.M. Torres Galvis, A.C. Koeken, J.H. Bitter, T. Davidian, M. Ruitenbeek, A.I. Dugulan, K.P. de Jong,  
11 Effect of precursor on the catalytic performance of supported iron catalysts for the Fischer–Tropsch  
12 synthesis of lower olefins, *Catalysis Today* 215 (2013) 95–102.
- 13 [23] A.A. Mirzaei, R. Habibpour, E. Kashi, Preparation and optimization of mixed iron cobalt oxide  
14 catalysts for conversion of synthesis gas to light olefins, *Applied Catalysis A: General* 296 (2) (2005)  
15 222–231.
- 16 [24] G.F. Botes, T.C. Bromfield, R.L. Coetzer, R. Crous, P. Gibson, A.C. Ferreira, Development of a  
17 chemical selective iron Fischer Tropsch catalyst, *Catalysis Today* 275 (2016) 40–48.
- 18 [25] Xu-Longya, Wang-Qingxia, Xu-Yide, Huang-Jiasheng, A new supported Fe-MnO catalyst for the  
19 production of light olefins from syngas. I. Effect of support on the catalytic performance, *Catal Lett* 24  
20 (1-2) (1994) 177–185.
- 21 [26] Xu-Longya, Wang-Qingxia, Xu-Yide, Huang-Jiasheng, Promotion effect of K<sub>2</sub>O and MnO additives on  
22 the selective production of light alkenes via syngas over Fe/silicalite-2 catalysts, *Catal Lett* 31 (2-3)  
23 (1995) 253–266.
- 24 [27] E. Iglesia, Synthesis and Catalytic Properties of Eggshell Cobalt Catalysts for the Fischer-Tropsch  
25 Synthesis, *Journal of Catalysis* 153 (1) (1995) 108–122.

- 1 [28] H. Schulz, G. Schaub, M. Claeys, T. Riedel, Transient initial kinetic regimes of Fischer–Tropsch  
2 synthesis, *Applied Catalysis A: General* 186 (1-2) (1999) 215–227.
- 3 [29] S. Golestan, A.A. Mirzaei, H. Atashi, Fischer-Tropsch synthesis over an iron-cobalt-manganese  
4 (ternary) nanocatalyst prepared by hydrothermal procedure: Effects of nanocatalyst composition and  
5 operational conditions, *International Journal of Hydrogen Energy* 42 (15) (2017) 9816–9830.
- 6 [30] T. Li, Y. Yang, C. Zhang, Z. Tao, H. Wan, X. An, H. Xiang, Y. Li, Effect of Manganese Incorporation  
7 Manner on an Iron-Based Catalyst for Fischer-Tropsch Synthesis, *Journal of Natural Gas Chemistry* 16  
8 (3) (2007) 244–251.
- 9 [31] S.S. Hla, G.J. Duffy, L.D. Morpeth, A. Cousins, D.G. Roberts, J.H. Edwards, D. Park, Catalysts for  
10 water-gas shift processing of coal-derived syngases, *Asia-Pacific Jnl of Chem. Eng* 5 (4) (2010) 585–  
11 592.
- 12 [32] G.P. van der LAAN, A.A.C.M. Beenackers, Hydrocarbon Selectivity Model for the Gas–Solid  
13 Fischer–Tropsch Synthesis on Precipitated Iron Catalysts, *Ind. Eng. Chem. Res.* 38 (4) (1999) 1277–  
14 1290.
- 15 [33] G.P. van der LAAN, A.A.C.M. BEENACKERS, Kinetics and Selectivity of the Fischer–Tropsch  
16 Synthesis: A Literature Review, *Catalysis Reviews* 41 (3-4) (1999) 255–318.
- 17 [34] M. Schaller, E. Reichelt, N. Fischer, M. Claeys, M. Jahn, Fischer-Tropsch to Higher Alcohols, in:  
18 DGMK Tagungsbericht 2017-2: Preprints of the Conference "Petrochemistry and Refining in a  
19 Changing Raw Materials Landscape", Dresden, 2017, pp. 99–106.
- 20 [35] M.E. Dry, Fischer-Tropsch synthesis over iron catalysts, *Catal Lett* 7 (1-4) (1990) 241–251.
- 21 [36] A.P. Steynberg, R.L. Espinoza, B. Jager, A.C. Vosloo, High temperature Fischer–Tropsch synthesis in  
22 commercial practice, *Applied Catalysis A: General* 186 (1-2) (1999) 41–54.
- 23 [37] D.J. Moodley, J. van de Loosdrecht, A.M. Saib, M.J. Overett, A.K. Datye, J.W. Niemantsverdriet,  
24 Carbon deposition as a deactivation mechanism of cobalt-based Fischer–Tropsch synthesis catalysts  
25 under realistic conditions, *Applied Catalysis A: General* 354 (1-2) (2009) 102–110.

- 1 [38] S.A. Eliason, C.H. Bartholomew, Temperature-programmed reaction study of carbon transformations  
2 on iron fischer-tropsch catalysts during steady-state synthesis, in: Catalyst Deactivation, Proceedings of  
3 the 7th International Symposium, Elsevier, 1997, pp. 517–526.
- 4 [39] R.B. Anderson, R.A. Friedel, H.H. Storch, Fischer-Tropsch Reaction Mechanism Involving Stepwise  
5 Growth of Carbon Chain, *The Journal of Chemical Physics* 19 (3) (1951) 313–319.
- 6 [40] P.J. Flory, Molecular Size Distribution in Linear Condensation Polymers 1, *J. Am. Chem. Soc.* 58 (10)  
7 (1936) 1877–1885.
- 8 [41] G.V. Schulz, Über die Beziehung zwischen Reaktionsgeschwindigkeit und Zusammensetzung des  
9 Reaktionsproduktes bei Makropolymerisationsvorgängen, *Zeitschrift für Physikalische Chemie* 30B (1)  
10 (1935).
- 11 [42] I. Puskas, R. Hurlbut, Comments about the causes of deviations from the Anderson–Schulz–Flory  
12 distribution of the Fischer–Tropsch reaction products, *Catalysis Today* 84 (1-2) (2003) 99–109.
- 13 [43] D. Förtsch, K. Pabst, E. Groß-Hardt, The product distribution in Fischer–Tropsch synthesis: An  
14 extension of the ASF model to describe common deviations, *Chemical Engineering Science* 138 (2015)  
15 333–346.
- 16 [44] E.S. Lox, G.F. Froment, Kinetics of the Fischer-Tropsch reaction on a precipitated promoted iron  
17 catalyst. 2. Kinetic modeling, *Ind. Eng. Chem. Res.* 32 (1) (1993) 71–82.
- 18 [45] R.A. Dictor, A.T. Bell, Fischer-Tropsch synthesis over reduced and unreduced iron oxide catalysts,  
19 *Journal of Catalysis* 97 (1) (1986) 121–136.
- 20 [46] D.B. Bukur, X. Lang, D. Mukesh, W.H. Zimmerman, M.P. Rosynek, C. Li, Binder/support effects on  
21 the activity and selectivity of iron catalysts in the Fischer-Tropsch synthesis, *Ind. Eng. Chem. Res.* 29  
22 (8) (1990) 1588–1599.
- 23 [47] E. Iglesia, Transport-enhanced alpha-olefin readsorption pathways in Ru-catalyzed hydrocarbon  
24 synthesis, *Journal of Catalysis* 129 (1) (1991) 238–256.

- 1 [48] H.M. Torres Galvis, A.C. Koeken, J.H. Bitter, T. Davidian, M. Ruitenbeek, A.I. Dugulan, K.P. de Jong,
- 2 Effects of sodium and sulfur on catalytic performance of supported iron catalysts for the Fischer–
- 3 Tropsch synthesis of lower olefins, *Journal of Catalysis* 303 (2013) 22–30.
- 4